Cranfield UNIVERSITY

Flow Studies at Hypersonic Speeds

Holger Babinsky

COA report No.9407
June 1991

College of Aeronautics
Cranfield University
Cranfield
Bedford MK43 0AL
England

College of Aeronautics Report No.
June 1991

Flow Studies at Hypersonic Speeds

Holger Babinsky

ISBN 1 871 564 778

£8

College of Aeronautics
Cranfield University
Cranfield
Bedford MK43 0AL
England

Acknowledgements

I would like to thank Prof. E. Messerschmid at the University of Stuttgart and Prof. J.L. Stollery at Cranfield Institute of Technology for their help and cooperation which made this work possible. I am especially grateful to Prof. J.L Stollery for his guidance and support as supervisor throughout this study.

I would like to express a special thanks to the technical staff at the College of Aeronautics who were essential to the experimental side of the project.

My final thanks is to Dipl.-Ing. H. Reissner whose grant enabled me to accept this opportunity to study in England.

Summary

Approximate methods for calculating the surface pressures including the effects of viscous interaction are introduced for laminar and turbulent boundary layers. Experiments were performed with various models taking schlieren pictures and pressure measurements. The flow over a two-dimensional compression corner showed transitional separation and were in agreement with other authors. The investigation of the flow over a delta wing with trailing edge flaps and body showed an influence of transition on the shape of the separated area, the pressure measurements were compared with various two-dimensional approximations. The experiments of a flow in the junction between a circular cylinder and a flat plate showed the influence of the sweep angle on the size of the separated region.

Es wurden verschiedene Näherungsmethoden zur Berechnung von Wanddrücken, unter Berücksichtigung der viskosen Interaktion, für laminare und turbulente Grenzschichten vorgestellt. Experimente wurden mit verschiedenen Modellen durchgeführt, wobei Schlieren-fotos und Druckmessungen gemacht wurden. Die Ergebnisse für eine 2-dimensionale Eckenströmung zeigen transitionelle Ablösung und sind in Übereinstimmung mit anderen Autoren. Die Strömung über einen Delta-Flügel mit Hinterkantenklappen und Rumpf zeigte einen Einfluß des Grenzschichtumschlages auf die Form des Ablösegebietes. Die Ergebnisse der Druckmessungen wurden mit verschiedenen 2-dimensionalen Abschätzungen verglichen. Die Untersuchung einer Strömung in der Kreuzung zwischen einem Kreiszylinder und einer ebenen Platte zeigte den Einfluß des Neigungswinkels auf die Länge des abgelösten Gebietes vor dem Zylinder.

Contents

	page
Notation	2
1. Introduction	4
2. Theoretical Considerations	5
2.1 Viscous Interaction	5
2.1.1 Laminar Boundary-Layer	7
2.1.2 Turbulent Boundary-Layer	10
2.2 Influence of Separation	13
3. Experimental Investigation	16
3.1 Experimental Facility	16
3.2 Models Tested	16
3.3 Pressure Measurements	17
4. Results and Discussion	19
4.1 Two-dimensional Corner Flow	19
4.2 Flow over a Flat Plate plus Cylinder	21
4.3 Flow over a Delta Wing with Trailing Edge Flaps	23
4.3.1 Schlieren Pictures	24
4.3.2 Pressure Measurements	25
5. Conclusions	29
6. References	31
7. Tables	35
8. Illustrations	37

Notation

x	distance along x-axis
y	distance along y-axis
y_w	body shape
y_e	effective body shape
L	reference length
$X = x/L$	dimensionless x
$Y = y/L$	dimensionless y
ξ	dummy variable along x-axis
δ^*	boundary layer displacement thickness
p	pressure
p_∞	free stream pressure
$P = p/p\infty$	pressure ratio
M_∞	free stream Mach number
$\gamma = c_p/c_v$	ratio of specific heats
T_w/T_o	ratio of wall temperature and stagnation temperature
C_∞	proportionality const. for linear viscosity law ($\mu/\mu_\infty = C_\infty\ T/T_\infty$)
$Re = \frac{u\ l}{\nu}$	Reynolds number
Re_L	Reynolds number at hinge line
$Re_\infty = \frac{u_\infty\ x}{\nu_\infty}$	free stream Reynolds number at distance x
$\bar{\chi} = \frac{M_\infty^3 \sqrt{C_\infty}}{\sqrt{Re_\infty}}$	laminar interaction similarity parameter
$\bar{\chi}_s = \left(\frac{C_\infty\ M_\infty^9}{Re_\infty}\right)^{2/7}$	turbulent strong interaction similarity par.
ϕ_i	angle to cause incipient separation at a compression corner
$k = M_\infty\ \alpha$	hypersonic similarity parameter

C_p		pressure coefficient
α		constant / angle of attack
β		constant / flap angle
R		constant
$\bar{R}$	= R/L	constant
A		constant
Q		constant
n		constant
k		constant

1. Introduction

Interest in hypersonic aerodynamics grew in the 1950's and 1960's with the beginning of the space program and later with the development of the Space-Shuttle. After almost 20 years of silence, the subject now experiences a revival due to the efforts in hypersonic transport vehicles, such as NASP, Hotol and Sänger.

Although modern computer models already achieve a three-dimensional viscous simulation of hypersonic flows /1,2/, a general understanding of the viscous interaction effects is still needed. Furthermore the effects of complex three-dimensional separations and transition are still not well understood and a great deal of further research seems necessary.

The present thesis investigates some of the above mentioned features experimentally on simple configurations and gives an overview on some approximate methods for the calculation of viscous interaction effects for laminar and turbulent flows. Special attention is given to the viscous effects on trailing edge flaps of a hypersonic vehicle, as it is well known that these effects can cause a loss of the effectiveness of such trailing edge controls /3/.

2. Theoretical Considerations

Due to aerodynamic heating, boundary-layers at hypersonic speeds can grow very strongly. Therefore the influence of the displacement thickness distorts the external flow field which in turn affects the boundary-layer. This phenomenon is called viscous interaction or pressure interaction. The local surface pressures can be very different from inviscid predictions, this effect has been first reported by Becker /4/, who measured pressures near the leading edge of a wedge. Theoretical investigations of this problem have been first carried out by Cheng /5/ who introduced the hypersonic similarity parameter $\bar{\chi}$ for laminar flow. By combining the approximate Newton-Busemann pressure law with a simple expression for the boundary-layer growth, Cheng could estimate the pressure distribution of flat plates at incidence in the strong interaction region close to the leading edge. Later Sullivan /6/ and Stollery /7/ introduced the tangent-wedge pressure law which expanded the applicability of the approximate viscous interaction methods to various body shapes. These methods also supplied solutions for regions far downstream of the nose, the weak interaction regime. Beyer /3/ carried out calculations for a flat plate fitted with trailing edge flaps, to investigate the influence of laminar viscous interaction on the pressure field of a typical re-entry vehicle. In this work similar calculations will be done for turbulent boundary-layers, using a method proposed by Stollery /8/. The theory for both laminar and turbulent viscous interaction will be introduced in 2.1. As these methods only allow predictions for attached flows, Chapter 2.2 will discuss the main effects of separation on corner flows and give an approximate method to predict the occurrence of separation.

2.1 Viscous Interaction

A simple example for the effect of viscous interaction is the

hypersonic flow over a flat plate at 0° incidence as shown in fig. 2.1:

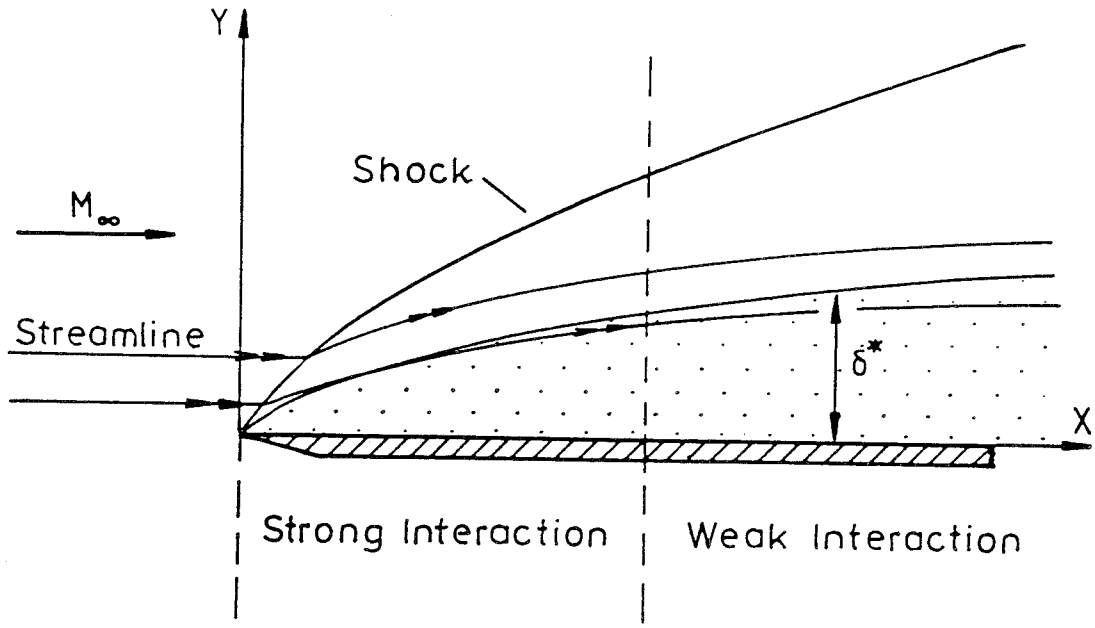

fig. 2.1 Hypersonic flow over a flat plate with a sharp leading edge

The strong growth of the boundary-layer near the nose changes the direction of the outer flow, hence a leading edge shock can be observed. The inviscid streamlines behind the shock are displaced upward, the pressure on the surface is well above the free stream pressure. This region is called the strong interaction region because the inviscid flow field is strongly affected by the growth of the boundary-layer.

Further downstream the rate of growth of the boundary-layer is much smaller, the streamlines are only weakly distorted, this region is called the weak interaction region. The pressure approaches its inviscid value in the limit of $x \rightarrow \infty$.

To determine the pressure distribution along a given body surface

$y_w = f(x)$ the following relations are needed:

The effective body shape has to be expressed in terms of the boundary-layer growth:

$$y_e = f(\delta^*) \tag{2.1}$$

The surface pressure has to be calculated as a function of the effective body shape:

$$p = f(y_e) \tag{2.2}$$

The boundary-layer growth as depending on the pressure:

$$\delta^* = f(p) \tag{2.3}$$

By combining analytic expressions for all three equations an approximate solution for the pressure and boundary-layer thickness of viscous flows over general body surfaces can be found.

For hypersonic flows equ. 2.1 can simply be written as:

$$y_e = y_w + \delta^* \tag{2.4}$$

Sullivan /6/, Stollery /7,8/ and Beyer /3/ achieved good results for interaction problems by using the tangent wedge law to express the surface pressure as a function of the effective body shape. The expression is (s. e.g. /9/):

$$\frac{p}{p_\infty} = 1 + \gamma\,(M_\infty\, y_e')^2 \left[\frac{\gamma+1}{4} + \left\{ \left(\frac{\gamma+1}{4} \right)^2 + \frac{1}{(M_\infty\, y_e')^2} \right\}^{1/2} \right] \tag{2.5}$$

As this study investigates laminar and turbulent boundary-layers two different expressions for equation 2.3 have to be found. The analysis for both cases can be found in the following chapters.

2.1.1 Laminar Boundary-layer

Following the work of Stollery /7/ and Beyer /3/, the local similarity solution for laminar boundary-layers can be used to express the displacement thickness of the boundary-layer:

$$\frac{M_\infty \delta^*}{x} = \frac{1}{2}(\gamma-1)\ 0.664 \left(1 + 2.6\frac{T_w}{T_o}\right) \bar{\chi} \left[\int_o^x \frac{p}{p_\infty}\frac{d\xi}{x}\right]^{1/2} \left(\frac{p}{p_\infty}\right)^{-1} \quad (2.6)$$

or

$$\frac{M_\infty \delta^*}{x} = \frac{A\,\bar{\chi}}{P}\left[\int_o^x P\frac{d\xi}{x}\right]^{1/2} \quad (2.7)$$

with

$$P = \frac{p}{p_\infty} \quad (2.8)$$

$$A = \frac{1}{2}(\gamma-1)\ 0.664 \left(1 + 2.6\frac{T_w}{T_o}\right) \quad (2.9)$$

and the viscous interaction parameter:

$$\bar{\chi} = \frac{M_\infty^3 \sqrt{C}}{\sqrt{Re_x}} \quad (2.10)$$

These equations are derived for a Prandtl number of unity, values of the constants for other Prandtl numbers can be found in /10/ and /6/. By introducing the new variable

$$R = \int P\,dx \quad (2.11)$$

and non-dimensionalising x with a characteristic length such as

$$X = x/L \quad (2.12)$$

where

$$L = A^2\,\bar{\chi}^2\,x \quad (2.13)$$

the following differential equation can be found (s. /7/):

$$\frac{dP}{dX} = \frac{P^2}{2R}\left\{1 + 2\,R^{1/2}\left[M_\infty \frac{dy_w}{dx} - Q\right]\right\} \quad (2.14)$$

where

$$Q = \frac{P - 1}{\gamma \left\{ 1 + \frac{\gamma+1}{2\gamma} (P-1) \right\}^{1/2}} \qquad (2.15)$$

These equation can be solved by using any kind of standard integration technique (e.g. Runge-Kutta), if suitable starting conditions are chosen. For sharp leading edges the pressure variation close to the nose depends only on the similarity parameter $\bar{\chi}$, hence the strong interaction solution can be used to provide initial values for P and R /7/. Expressed in the nondimensionalised variables, the initial pressure for a starting point X_o is:

$$P_o = \frac{3}{4} \sqrt{\gamma\,(\gamma-1)}\; X_o^{-1/2} \qquad (2.16)$$

As

$$R_o = \int_0^{X_o} P \, dX \qquad (2.11)$$

then

$$R_o = \frac{3}{2} \sqrt{\gamma\,(\gamma-1)\, X_o}$$

or

$$R_o = 2\, X_o\, P_o \qquad (2.17)$$

In this study the pressure variation over a flat plate at incidence fitted with a trailing edge flap was computed using the introduced model. The integration of equ. 2.11 and 2.14 was carried out using a variable step Runge-Kutta-algorithm. Using a variable step algorithm it was possible to capture the change of y'_w exactly at the hinge line, independent from the chosen step size. The program was written in ACSL (Advanced Continuous Simulation Language) and run on an IBM-compatible PC. The agreement of the predicted pressures with experimental results is good, regarding the simplicity of the analysis. Examples and further details are given in /3/ and /7/.

2.1.2 Turbulent Boundary-layer

Stollery and Bates give a general expression for the boundary-layer displacement thickness of turbulent flows /8/:

$$\delta^* = A \frac{M_\infty^{4/5} C_\infty^{1/5}}{Re_\infty^{1/5}} \times \frac{\left[\frac{1}{x} \int_o^x P^\alpha d\xi \right]^{4/5}}{P^\beta} \qquad (2.18)$$

with

$$A = 0.051 \frac{1 + H_i \, T_w/T_o}{(1 + 2.5 \, T_w/T_o)^{3/5}} \qquad (2.19)$$

$$\alpha = \frac{1}{7} \left(\frac{23}{4} - \frac{5}{4} H_i \frac{T_w}{T_o} \right) \qquad (2.20)$$

$$\beta = \frac{1}{7} \left(6 - H_i \frac{T_w}{T_o} \right) \qquad (2.21)$$

This expression was derived by assuming local flat plate similarity and using Eckert's reference enthalpy method. Details are given in /11/.

By defining a new variable

$$R = \int P^\alpha dx \qquad (2.21)$$

and differentiating with respect to x, the following expression can be obtained

$$\frac{d\delta^*}{dx} = B \left[\frac{4}{5} P^{\alpha-\beta} R^{-1/5} - b \, R^{4/5} P^{-(1+\beta)} \frac{dP}{dx} \right] \qquad (2.22)$$

Rearranging 2.5

$$M_\infty \frac{dy_e}{dx} = \frac{P - 1}{\gamma \left\{ 1 + \frac{\gamma+1}{2\gamma} (P-1) \right\}^{1/2}} \equiv Q \qquad (2.23)$$

and combining with 2.4 differentiated with respect to x gives

$$\frac{d\delta^*}{dx} = \frac{Q}{M_\infty} - \frac{dy_w}{dx} \qquad (2.24)$$

2.22 and 2.24 can be combined and written as

$$\frac{dP}{dx} = \frac{4\ P^{\alpha+1}}{5\ \beta\ R} - \left(\frac{u_\infty}{M_\infty^4\ C_\infty\ \nu_\infty}\right)^{1/5} \frac{1}{A}\ \frac{P^{\beta+1}}{\beta\ R^{4/5}} \left(\frac{Q}{M_\infty} - \frac{dy_w}{dx}\right) \qquad (2.25)$$

After normalizing x and R with a reference length L

$$X = \frac{x}{L} \qquad (2.26)$$

$$\bar{R} = \frac{R}{L} \qquad (2.27)$$

where

$$L = A^5 \frac{M_\infty^9\ C_\infty}{Re_x}\ x \qquad (2.28)$$

equation 2.25 can finally be written

$$\frac{dP}{dX} = \frac{P}{\beta\ \bar{R}} \left(\frac{4}{5} P^\alpha - \bar{R}^{1/5}\ P^\beta \left(Q - M_\infty \frac{dy_w}{dx}\right)\right) \qquad (2.29)$$

and 2.21 changes to

$$\bar{R} = \int_0^X P^\alpha\ d\xi \qquad (2.30)$$

2.29 and 2.30 now define a set of differential equations that can be integrated in the same fashion as for the laminar case. To obtain suitable starting conditions it is sufficient to calculate the flat plate case at 0° incidence ($dy_w/dx = 0$). It is assumed that the pressure variation in the nose region obeys a power law:

$$P = k\ X^n \qquad (2.31)$$

then

$$\bar{R} = \frac{k^\alpha}{\alpha n+1} X^{\alpha n+1} \qquad (2.32)$$

After substituting 2.31 and 2.32 in 2.29 and assuming a strong interaction ($P \gg 1$) the result is

$$\frac{dP}{dX} = \frac{4k(\alpha n+1)}{5\ \beta} X^{n-1} - \frac{(\alpha n+1)^{4/5} k^{1+\beta-4\alpha/5}}{\beta} \sqrt{\frac{2\ k}{\gamma(\gamma+1)}}\ X^{n\beta+n-4\alpha n/5-4/5+n/2}$$

Comparing this with 2.31 and using

$$5\ \beta - 4\ \alpha = 1 \qquad (2.33)$$

gives

$$n = -\frac{2}{7} \tag{2.34}$$

and

$$k = \left(\frac{\gamma(\gamma+1)}{2}\right)^{5/7}\left(\frac{6}{7}\right)^{10/7}\left(1 - \frac{2}{7}\alpha\right)^{-8/7} \tag{2.35}$$

Introducing the turbulent similarity parameter for strong interaction as derived in /8/

$$\bar{\chi}_s = \left(\frac{M_\infty^9 C_\infty}{Re_{x\infty}}\right)^{2/7} \tag{2.36}$$

the strong interaction solution is:

$$P = \left(\frac{6}{7}\right)^{10/7}\left(\frac{\gamma(\gamma+1)}{2}\right)^{5/7}\left(\frac{5}{98}\left(15 + H_i \frac{T_w}{T_o}\right)\right)^{-8/7} A^{10/7}\,\bar{\chi}_s \tag{2.37}$$

This equation shows that the pressure in the strong interaction region is directly proportional to the strong interaction parameter. A similar result obtained with a simpler expression for the displacement thickness can be found in /8/. Analogous to the laminar calculation, this expression can now be used to provide initial values for the integration of 2.29 and 2.30. The method used to obtain some of the results below is similar to the code for the laminar case.

Fig. 2.2 shows a calculated pressure profile for a flat plate at 0 degree incidence and 20 degrees flap angle. The Mach number is 9.22, the Reynolds number at the hinge line is $2.37 \cdot 10^7$. Also indicated are experimentally measured pressures for this case /12/.

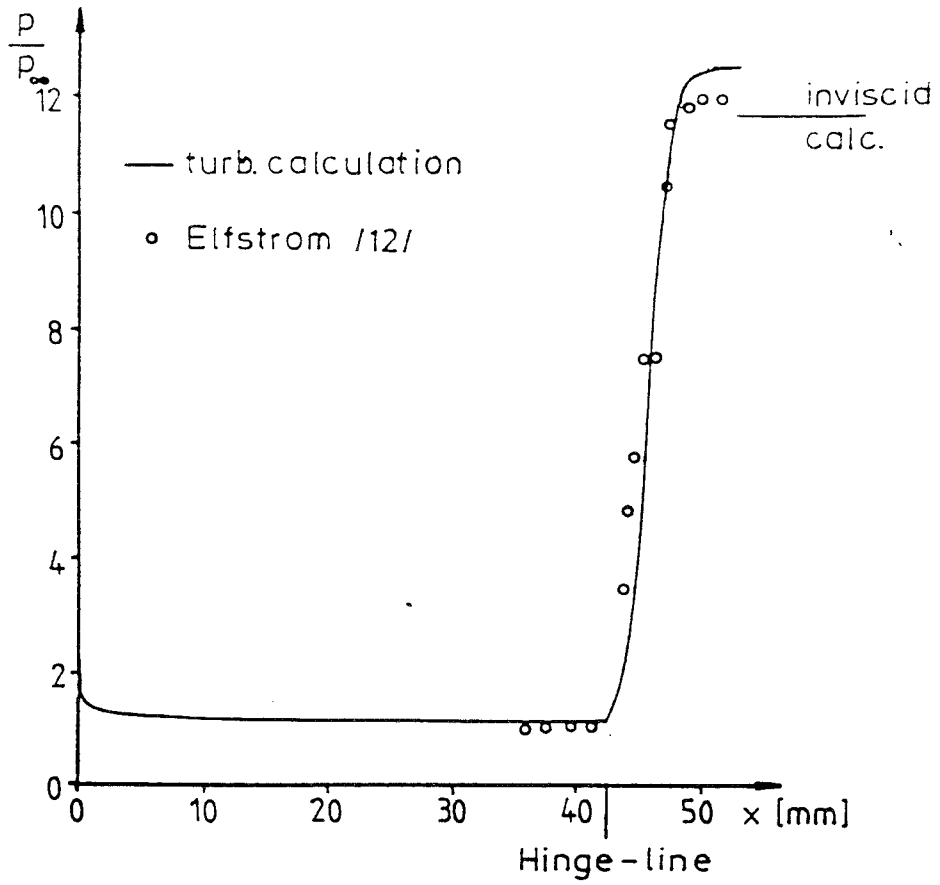

fig. 2.2 Turbulent pressure distribution for the flow over a flat plate with a 15° compression corner

It can be seen that the computed pressure indicates a peak at the leading edge, this is due to the boundary-layer growth which gives rise to a shock-wave followed by an expansion fan. The agreement between the prediction and the measurement for the pressure rise at the flap is relatively good, although the theory is not capable of predicting any upstream influence. Additionally, it is not possible to calculate separated flows, as the boundary-layer profiles are assumed to be reasonably similar.

2.2 Influence of Separation

In the previous chapters some examples for typical pressure profiles of compression corner flows have been given. In all cases a strong increase of pressure in the region of the hinge line can be noticed. If the angle of the compression corner or the trailing edge flap

becomes too steep, the pressure rise will eventually cause a separation of the boundary-layer. A typical flow pattern for this case is sketched in fig. 2.3.

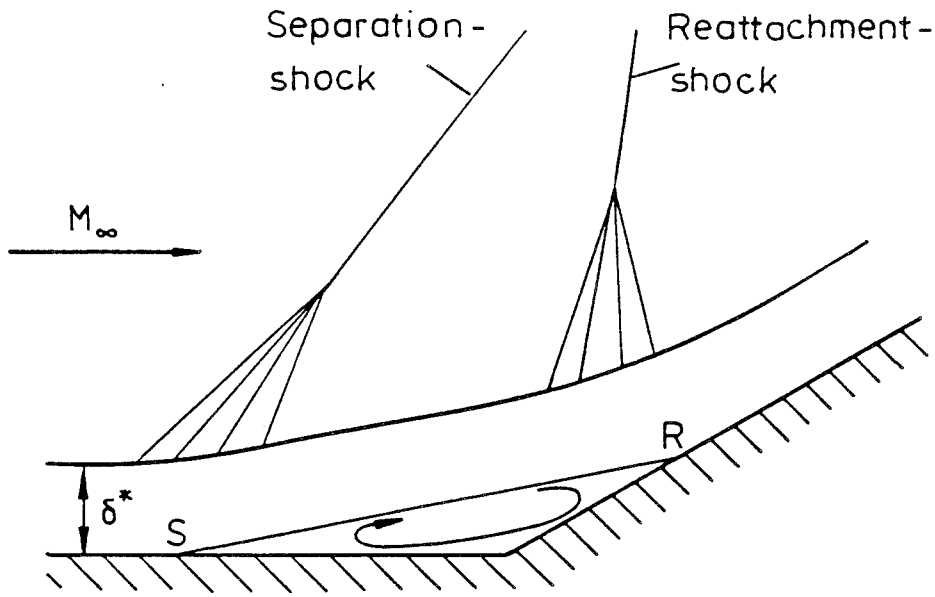

fig. 2.3 Flow pattern for separated corner flows

At the separation point a compression fan can be noticed forming a first strong shock at a certain distance from the wall. The boundary-layer changes itself into a free shear-layer. The pressure rises through this shock and reaches an almost constant value, the so-called plateau pressure. At the reattachment point the boundary-layer thins and a second compression-fan is generated. The pressure distribution shows a second rise and usually reaches a peak value above the inviscid wedge prediction, further downstream.

The necessary angle to cause separation is much larger for turbulent boundary-layers than in the laminar case. The fluctuations in a turbulent boundary-layer provide a mechanism for mixing with the energy of the outer flow, therefore it is more robust and less likely to separate from the surface under a positive pressure gradient than a laminar boundary-layer. For the laminar case a big amount of experimental work has been carried out (e.g. /13/,/14/,/15/,/16/) and

empirical relations have been found to predict the wedge-angle to cause separation. Needham /14/ derived the following expression by using a simple order of magnitude analysis :

$$M_\infty \phi_i = 80 \bar{\chi}^{1/2} \tag{2.38}$$

where $\bar{\chi}$ is the interaction parameter for laminar flow

$$\bar{\chi} = \frac{M_\infty^3 \sqrt{C}}{\sqrt{Re_L}} \tag{2.39}$$

Ginoux /17/ obtained a similar expression which seems to fit better to some of the at lower M-numbers obtained results:

$$\phi_i = \frac{36.63 \sqrt{M_\infty}}{Re_L^{1/4.5}} \tag{2.40}$$

where Re_L is the value of the Reynolds number at the hinge-line.
To compare these equations, 2.38 can also be written as

$$\phi_i = \frac{80 \sqrt{M_\infty}}{Re^{1/4}} \tag{2.41}$$

Both expressions are shown in fig. 4.2, together with some experimental data.

3. Experimental Investigation

The experimental work studied the applicability of the approximate viscous interaction theory, described in the previous chapters, for real delta-wing flows. Furthermore some experiments were carried out to investigate the flow-patterns for configurations with a strongly 3-dimensional separation to achieve an understanding of this phenomenon.

3.1 Experimental Facility

All experiments have been carried out in the hypersonic gun tunnel of the College of Aeronautics at the Cranfield Institute of Technology. This tunnel has formerly been at the Imperial College in London and a detailed description is given in /18/. This facility is an intermittent, free-piston, blow down tunnel with a running time of approximately 40 ms. A light aluminium piston is driven by compressed air at a drive pressure of 2000 psia (137 bar), giving an initial test gas at a total temperature of 1290 K and a total pressure of 1455 psia (100 bar). After the expansion in a contoured nozzle, the flow accelerates to a Mach number of 8.2 at free stream conditions of p_∞ = 0.127 psia (0.009 bar) and T_∞ = 89.3 K. The flow is uniform within the test-section having a useful core of about 0.12 - 0.15 m. The length of the working section is 0.20 m.

3.2 Models Tested

The first model used in this study was a flat plate with a span of 5 inch (0.127 m) and a chord of 8 inch (0.203 m) as shown in figure 3.1. The leading edge was ground to a 10° bevel angle and honed to a sharp edge. This model could be mounted at any incidence between 0° and 30°. It could either be fitted with wedges of 1.73" chord (0.044 m) and 5" span, or with circular cylinders of a diameter

of 1 inch (0.02 m). Wedges were used with an angle of 5°, 10° and 30°, the cylinders could be mounted at angles of 0°, 15°, 30° and 45° to the vertical of the plate (s. fig. 3.2), either facing forwards or backwards.

The second model used was a delta wing with fuselage and trailing edge flaps as shown in fig. 3.3. Possible flap angles were 0°, 10° and 20°. The model had an overall length of 20.5 cm and a wingspan of 12 cm. The wing thickness was 3 mm with knife edges at the leading and trailing edge. The model was mounted from a support attached at the top of the fuselage towards the rear of the model. Analogous to the flat plate, the model could be fitted at various incidences between 0° and 30°. After the taking of the schlieren pictures, the model was fitted with pressure transducers at the under surface as described in the following section.

3.3 Pressure measurements

The under surface of the delta wing model was fitted with 29 pressure tappings as shown in fig. 3.4. Although the estimated free-stream pressure was as low as 0.127 psia a range of the pressure transducers of 0 - 20 psi was chosen to avoid overload at high angles of attack. For the experiments six absolute, piezo-resistive transducers, Kulite LQ-080-25A, were used. To obtain accurate results within the short running-time of the tunnel, the physical distance between the transducers and the pressure tappings was kept as short as possible. Therefore the transducers were mounted in a special housing in the fuselage of the model. To interchange the connections to the different pressure tappings a system of rubber and metal tubes with a diameter of 0.5 mm was used. This method avoided moving the transducers themselves, so that damage could be prevented. By mounting the metal tubes within the wing and keeping the rubber tubes short, it was possible to keep most of the connections within the

body profile. This minimised any disturbance to the external flowfield. Furthermore all the installations were on the upper surface of the wing, well behind the leading edge so that the influence on the lower surface flow could be assumed to be minimal. Information on pressure transducers and response time can be found in /19/.

As most of the data were expected to be below 5% of the full range it was necessary to keep the noise ratio as low as possible. Therefore the transducers were supplied with a battery power supply, being stabilized to 5 volts. The signal was then amplified, using an amplifier Fylde M14DS, and connected to a Datalab DL2808 transient recorder. The sample rate was adjusted to 10 μs. Finally the traces were plotted out on a chart recorder. To overcome the effects of temperature-drift the atmospheric and the vacuum pressure in the working section was recorded and plotted out before every run. From static calibrations of the transducers the response between 0 and 15 psi was found to be linear. Therefore the two outputs obtained were sufficient to calibrate the transducers. This procedure was performed independently for every transducer.

4. Results and Discussion

4.1 Two-dimensional corner flow

To obtain schlieren pictures of a corner flow the flat plate model was fitted with different wedges (s. fig. 3.1). All pictures were taken on Polaroid film (Type 47, 3000 ASA), therefore only photocopies can be shown in this report. An investigation by Pate /20/ showed that three-dimensional effects on the behavior of the separated region only become significant when the aspect ratio of the separated region is smaller then 2. Needham /14/ confirmed these results for different Mach numbers. Therefore the results obtained in this study are assumed to be two-dimensional.

Experiments were performed with wedges of 5, 10 and 30 degrees at incidences of 0, 5 and 10 degrees. Some of the results are shown in fig 4.1, where α indicates the angle of attack and β stands for the wedge angle. The 30° wedge could only be used at 0° incidence, an angle of attack of 5° already caused a blockage in the tunnel.

The Reynolds-number at the hinge line was $1.3 \cdot 10^6$ for 0° incidence. Due to the stronger leading edge shock the conditions at the hinge-line change to:

$M = 7.0 \quad Re_L = 2.2 \cdot 10^6 \quad$ for 5° incidence
$M = 5.9 \quad Re_L = 2.3 \cdot 10^6 \quad$ for 10° incidence.

The case for 0° incidence / 30° flap, shows an interesting flow pattern which can be compared to the sketch in fig. 2.4. Behind the leading edge shock a laminar boundary layer can be observed. At approximately half the distance to the compression corner the flow separates and the separation shock can clearly be seen. The laminar boundary-layer has now changed to a laminar shear-layer. The schlieren picture indicates a possible transition but further

investigation is needed to confirm this assumption. On the wedge, a reattachment of the shear-layer can be observed. The reattachment shock can be seen and this crosses the separation shock near the end of the wedge.

It can be seen that the separation and reattachment shock are useful indications of a separated region. The boundary-layer itself is sometimes not as easy to see and, in the case of small separated region, does not clearly indicate the separation. A good example is the 10° corner flow at 5° incidence (fig. 4.1). The boundary-layer appears to be laminar and attached along the whole length of the picture. By looking closely at the corner region and comparing the picture to a non-separated case as for example 10°incidence/5°wedge two shocks can be noticed, indicating a very small separated region.

The results are summarized in table 1. It indicates separated or attached flow for all tested configuration. α is the incidence and β is the wedge angle.

The only suggestion of transition was the appearance of ripples in the free shear layer for the $\alpha = 0^{\circ}$, $\beta = 30^{\circ}$ configuration (see fig. 4.1).

In chapter 2.2 formulas were introduced to predict laminar separation. Fig. 4.2 shows values for the angle to cause separation (α_i) as a function of the Re-number at the hinge line, calculated by using equ. 2.38 and equ. 2.40 as well as some experimental results /13/. As this study investigated only few different wedge angles, exact results for the angle to cause separation can not be given. Nevertheless it can be said that separation occurs for values between the angles for separated and attached flow and therefore the largest angle to show attached flow is included in fig. 4.2. Some of the obtained results are in the transitional regime. This supports the observation of a transition in the free shear layer in the case of

the 30° wedge. Although none of the other schlieren pictures showed signs of a transition in the boundary layer, a transitional behavior is found in the separation. Similar observations have been made by other authors e.g. /21/.

The methods described in chapter 2.1 were used to calculate the pressure and boundary-layer thickness distributions as shown in fig. 4.3. The flat plate with a 5° wedge has been calculated for laminar and turbulent boundary-layer at incidences of 0°, 5° and 10°. All cases show that the turbulent boundary-layer is thicker than the laminar boundary-layer, although there is a region near the leading edge where the laminar layer grows stronger. For increasing angles of attack the boundary-layers become thinner, due to the higher pressure behind the leading edge shock. This seems to affect the laminar layer more than the turbulent layer. The pressure distributions show only little influence of the viscous effects, the pressure peak at the leading edge is in a very narrow region and the pressure along the flap reaches its final value although the flap is only short. This is very different to the viscous effects for thick boundary-layers as calculated by Beyer /3/ for a re-entry configuration. With increasing angle of attack the viscous effects become even less important, as the boundary-layer thickness decreases. As the decrease of the boundary-layer thicknes due to the higher pressure is more important in the laminar case, the viscous effects are less dominant for the laminar boundary-layer (see fig. 4.3, α=10°).

4.2 Flow over a Flat Plate plus Cylinder

After the investigation of a 2-dimensional flow field a highly three-dimensional separated flow has been studied. The problem of the interaction of a flat plate boundary layer with the bow shock of a blunt body, is very important in hypersonic flows. These problems can be observed at fin/body junctions or in intake flows where struts are

needed to provide static support. In the area of supersonic combustion (Scram-jet) blunt struts may be necessary to inject fuel and keep the combustion-zone stable.

All these problems have the common feature of a large separated region, caused by the interaction of the bow shock ahead of the blunt nose (or cylinder) with the boundary-layer along the surface perpendicular to it. The size of the separated region can be decreased by sweeping the cylinder backwards. For intake flows this has the disadvantage that a forward facing configuration can not be avoided on the opposing side of the intake.

To investigate this type of configuration a circular cylinder was mounted on the surface of the flat plate. To show the influence of the sweep angle different cylinders were available (s. fig. 3.2). The flow field was studied by schlieren pictures.

Fig. 4.4 shows the results for a perpendicular cylinder and for sweep angles of ±15, ±30 and ±45 degrees. In the case of the cylinder at 0° a large laminar separation is observed starting about 3cm behind the leading edge. The separation shock crosses through the leading edge shock shortly before both reach the bow shock in front of the cylinder. Although the flow pattern is highly three-dimensional the schlieren pictures provide a useful tool to judge the separation. It can be assumed that the separated region is much shorter towards the sides of the flat plate, the pictures only indicate the beginning of the separation along the center-line.

By sweeping the cylinders backwards the expected effect of a decreasing separation is observed. At 45° the separated region has almost completely vanished, its expanse along the center-line is only about 2cm.

All pictures for forward facing cylinders show a separation starting

at about the same point, very close to the leading edge. The separation does not grow closer to the nose, a possible explanation is the ability of the boundary-layer to withstand a pressure rise, as it is still very thin and short. To be able to observe differences in the effect of the different forward sweep-angles , a longer flat plate is needed to allow a bigger separation. Another possibility could be, to use cylinders of a smaller diameter. Because of lack of time and in order not to deviate from the main objectives of this project, these experiments were not performed.

It can be concluded that backward facing cylinders have the expected positive effects. The sweep angle of 45° showed the best results, causing only a very small separated region. Forward facing cylinders lead to a bigger separation, a difference between various sweep angles could not be found, as the flat plate proved to be too short.

4.3 Flow over a Delta Wing with Trailing Edge Flaps

The main aim of this study was to investigate the flow field of a simple aircraft-like configuration as shown in fig. 3.3. Similar investigations have been carried out by various authors, mostly for delta wings with trailing edge flaps /22/,/16/,/23/,/24/. In earlier years these studies concentrated mainly on re-entry vehicles and therefore covered blunt leading edges and high angles of attack. Investigations of hypersonic aircraft configurations including a fuselage have been investigated more recently, for example /25/ and /26/.

Rao carried out an investigation of the flow around a delta wing with trailing edge flaps and a sharp leading edge /27/. By comparing two- and three-dimensional experiments he showed that two-dimensional predictions can give good agreement under certain conditions. This was valid for attached or mildly separated flows at smaller angles of

attack. A prediction for incipient separation using the two-dimensional results showed good agreement for turbulent boundary-layers. For laminar flows the flap angles to cause separation were larger than in the two-dimensional case. Transition was found to occur earlier on the delta wing than on the flat plate and proved to have a great impact on the shape of the separated region. The present study tried to obtain comparable results for a delta wing fitted with a body.

4.3.1 Schlieren Photographs

Schlieren pictures were taken for all flaps (0°,$10^{\circ}$and 20°) at incidences of 0,5,10,15 and 20 degrees. For the case with 0° incidence, the Re-number at the hinge line is $1.5 \cdot 10^{6}$, using the centre-cord. This is slightly larger than for the 2-dimensional corner flow studies in chapter 4.1. As any other Re-number away from the centre-line is smaller than this value, it seems reasonable to compare the results.

Fig. 4.5 shows some of the schlieren pictures for the delta wing model. Due to the strong three-dimensionality (unequal boundary-layer thickness across the flow and complex shape of the separation) it is more difficult to detect separated regions at the lower surface. Nevertheless, it is possible to detect the shock ahead of the hinge line, indicating separation.

Table 2 gives an overview of the observed separation for the different configurations.The results are in agreement with the results obtained for the flat plate in chapter 4.1. Therefore by using the flow conditions along the centre-line, a reasonable indication for the appearance of separation can be given from two-dimensional data.

Naturally the schlieren pictures provide no information on the

three-dimensional shape of the separated region. This can be achieved by using pressure measurements on the lower surface of the delta wing.

4.3.2 Pressure Measurements

Due to the short time available, pressure measurements were only performed on one configuration. The model was put at an incidence of 15° and the 20° flap was used. A schlieren picture was taken to confirm that the model modifications did not cause a severe change in the flow field.

The shape of the recorded transducer signals was dependant on the location of the connected tapping. Two typical examples are shown in fig. 4.6. The measurement near the front of the fuselage (I) was recorded using only a short physical distance between the tapping and the transducer. The transducer was mounted just above the tapping. Accordingly, it shows a better time response than signal II which is a tapping near the outer edge of the flap. In this case the connection to the pressure tapping consisted of a 60 mm metal tube within the wing and a rubber tube of about 30 mm length. It can be noticed that a significant damping exists in the signal, the stationary period is only very short. Therefore, the results obtained on the flap area have to be treated with care. To obtain a higher accuracy for the pressures in these areas, measurements were repeated up to 4 times and a mean value was calculated. Sometimes a spread between the results of up to 40% could be noticed. By using different transducers the values could differ even further. This suggests that the static calibration as described in 3.3 is not sufficient and an independent dynamic calibration for every transducer needs to be carried out. Another source for the great spread in the results could be an unstable separation pattern on the flap. Further experiments are needed to investigate this problem.

During some of the first runs, very high pressures were recorded on the outer edges of the wing. This phenomenon disappeared after moving the model further forward in the working section. All results used in this study were achieved in this forward position.

Fig. 4.7 shows the results obtained for pressure tappings mounted along the centre-line (see also fig. 4.8). The pressure rises slightly from the cone to the wing-surface towards the hinge-line. The pressure-distribution at the hinge-line suggests a small separated area with the pressure rising steeply on the flap. Some results of two-dimensional calculations are also shown in this picture. The tangent-cone approximation was calculated with an analytic expression derived by Rasmussen, using the small disturbance theory /9/:

$$\frac{C_p}{\theta_c^2} = 1 + \frac{(\gamma+1)K^2 + 2}{(\gamma-1)K^2 + 2} \ln\left(\frac{\gamma+1}{2} + \frac{1}{K^2} \right) \qquad (4.1)$$

where θ_c is the cone angle and K is the hypersonic similarity parameter $M_\infty \cdot \theta_c$. To obtain the pressure relation $P = p/p_\infty$, the following relation can be used:

$$P = \frac{1}{2} \gamma C_p M_\infty^2 + 1 \qquad (4.2)$$

This calculation gives a good predictions of the pressure on the centre-line of the lower surface. The tangent wedge approximation gives too high a value for this pressure but too small a value for the flap pressure. This is not surprising as the flap pressure is created by two shocks, whereas the tangent-wedge value gives the pressure after a single shock. The tangent-cone method gives an even smaller value for the flap pressure, for the same reasons. A reasonable inviscid approximation for the flap pressure was made by using the tangent cone result and assuming a two-dimensional shock with a deflection of 20°. Similar results can be found in /27/.

Naturally the inviscid calculations can not predict the pressure rise near the hinge-line. Two calculations with the programs described in 2.1 have been made to give results of viscous interaction methods. Both, the laminar and the turbulent computation are shown in fig. 4.7. The laminar calculation shows a smaller influence of the viscous effects, the turbulent result gives a better prediction for the slope of the pressure rise on the flap. Both methods can not predict the measured upstream influence or the plateau for the separated region. As the tangent wedge rule is used to calculate the pressures, both methods give too high a value for the center-line pressure upstream of the flap.

Fig. 4.8 gives the pressures recorded on the wing, along lines parallel to the centre-line, fig. 4.9 gives lines perpendicular to it. These results have been obtained under the assumption of symmetrical flow. It can be seen that the separation is larger on the wing than on the centre-line. This is also supported by the pressure contours in fig. 4.10. From fig. 4.8 can be seen that the flow near the outer edge of the wing is almost completely attached. These observations were used to sketch the separated area shown in fig. 4.10. The location of the separation-point, as seen from the schlieren pictures is also marked.

In conclusion it can be stated that the separation has a highly three dimensional shape. The relatively short separation near the centre-line is probably due to an earlier transition forced by the forebody. On the wings, were the flow is likely to be completely laminar, the separation is much larger. Close to the edges of the wing the boundary-layer is less likely to separate. The Re-number is lower, the momentum loss is small and hence the layer is more resistant to laminar separation (see fig. 4.2). A similar result was

obtained by Rao /27/ for delta wings without a fuselage, as shown in fig. 4.11.

5. Conclusions

The main objective of this study was to gain knowledge of the flow over the lower surface of a simple hypersonic vehicle fitted with trailing edge flaps. As three-dimensional separation was expected to occur, some experiments on different configurations, showing this phenomenon, were performed.

The flow over a flat plate fitted with a cylinder showed a strong influence of the sweep angle on the size of the separated region. A forward sweep increases this area, a backward sweep decreases it.

Experiments of a two-dimensional compression corner at different incidences and corner angles gave information on laminar and transitional separation in agreement with other authors. By comparing these results with the flow over the delta wing with flaps, it was found that some indication of separation was possible by using the two-dimensional results applied to strips parallel to the centre line.

The three-dimensional shape of the separated area proved to be influenced strongly by an early transition near the centre line of the flow. Therefore the separated region on the middle of the wing was shorter than further outboard. On the outer edges of the wing the separated length decreased again.

Some work has been done to introduce approximate methods to calculate the effects of viscous interaction on the pressure distribution along curved surfaces for laminar and turbulent boundary-layers. The agreement of the calculated data with the experimental results of the delta wing was only moderate, as other effects dominated the flow field.

To improve the results obtained further experience on the use of the

pressure transducers is needed. A dynamic calibration could prove useful. The influence of the tubing used to connect the pressure tappings with the transducers also needs further investigation.

The calculated data should be compared to measurements for an attached flow to give a better judgment on the accuracy of the method.

References

/1/ Shang J.S., Scherr S.J., 'Navier-Stokes Simulation for a Complete Re-Entry Configuration'
Journal of Aircraft 23, no.12, 1986

/2/ Hollander H., Marmignon C., 'Navier-Stokes High Speed Flow Calculations by an Implicid Non-Centre Method'
AIAA 89-0282

/3/ Beyer U., 'Control Effectiveness of Flaps at Hypersonic Speeds'
MSc Thesis, Cranfield Institute of Technology, 1988

/4/ Becker J.V., 'Results in Recent Hypersonic an Unsteady Flow Research at the Langley Aeronautical Laboratory'
Journal of Applied Physics 21, no.7, 1950

/5/ Cheng H.K., Hall J.G., Golian T.C. and Hertzberg A.
'Boundary-Layer Displacement and Leading Edge Bluntness Effects in High-Temperature Hypersonic Flow'
Journal of Aeronautical Sciences 28,1961

/6/ Sullivan P.A., 'On the Interaction of a Laminar Hypersonic Boundary-Layer and a Corner Expansion Wave'
UTIAS TH.129, 1968

/7/ Stollery J.L., 'Hypersonic Viscous Interaction on Curved Surfaces'
Journal of Fluid Mech. 43, 3, 1969

/8/ Stollery J.L., Bates L., 'Turbulent Viscous Interaction'
Journal of Fluid Mech. 63, 1, 1974

/9/ Anderson ; J.D., 'Hypersonic and High Temperature Gas Dynamics'
McGraw-Hill, 1989

/10/ Dewey C.F., 'The Use of Local Similarity Concepts in Hypersonic Viscous Interaction Problems'
AIAA-Journal 1

/11/ Stollery J.L., Imperial College Aero. Rep., no 73-04, 1973

/12/ Elfstrom G.W., Journal of Fluid Mech. 53, 1972

/13/ Holden M.S., 'Leading Edge Bluntness and Boundary Layer Displacement Effects on Attached and Separated Laminar Boundary Layers in a Compression Corner'
AIAA paper 68, 1968

/14/ Needham D.A., 'Laminar Separation in Hypersonic Flow'
PhD Thesis, University of London, 1965

/15/ Miller D.S., Hijman R., Childs M.E., 'Mach 8 to 22 Studies of Flow Separations Due to Deflected Control Surfaces'
AIAA-J. 2, 1964

/16/ Giles H.L., Thomas J.W., 'Analysis of Hypersonic Pressure and Heat Transfer Tests on a Flat Plate with a Flap and a Delta Wing with Body and Elevon, Fins and Rudder'
NASA CR-536, 1966

/17/ Ginoux J.J., VKI-TN 60

/18/ Stollery J.L., Maull D.J., Belder B.J., 'The Imperial College Hypersonic Gun Tunnel'
Journal of the Royal Aeron. Soc. Vol 64, 1964

/19/ Bynum D.S., Ledford R.L., Smotherman W.E., 'Wind Tunnel Measuring Techniques'
AGARD-AG-145-70

/20/ Pate S.R., 'Investigation of Flow Separation on a Two Dimensional Flat Plate Having a Variable Span Trailing Edge Flap at M = 3 and M = 5'
AEDC-TDR-64-14

/21/ Ginoux J.J., VKI-TN 30 and VKI TN 47

/22/ Nagel A.L., Fitzsimmons D.H., Doyle L.B., 'Analysis of Pressure and Heat Transfer on Delta Wings with Laminar and Turbulent Boundary-Layers'
NASA CR-535, 1966

/23/ Dunavant J.C., 'Investigation of Heat Transfer of Highly Swept Flat and Dihedraled Delta Wings at Mach Numbers of 6.8 and 9.6 and Angles of Attack to 90°'
NASA TN X-688

/24/ Collins D.C., 'A Hypersonic Windtunnel Study of a Thick Delta Wing'
A.R.L Aero.Note 232, 1964

/25/ Richardson P.F., Parlette E.B. et al, 'Comparison Between Experimental and Numerical Results for a Research Hypersonic Aircraft'
Journal of Aircraft Vol.27, No.4, 1990

/26/ Reubush D.E., 'Pressure and Heat Transfer Investigation of a Modified NASP Baseline Configuration at M=6'
AIAA Paper No. 89-0246, 1989

/27/ Rao D.M., 'Hypersonic Control Effectiveness Studies on Delta Wings with Trailing Edge Flaps'
PhD Thesis, University of London, 1970

7. Tables

α \ β	0°	5°	10°	30°
0°	attached	attached	separated	separated
5°	attached	attached	separated	not tested
10°	attached	attached	separated	not tested

Table 1 Results for flat plate fitted with wedges at various angles of attack

α \ β	0°	10°	20°
0°	attached	separated	separated
5°	attached	separated	separated
10°	attached	separated	separated
15°	attached	not tested	separated
20°	attached	attached	blockage

Table 2 Results for flow over delta wing at different incidences and flap angles

8. Illustrations

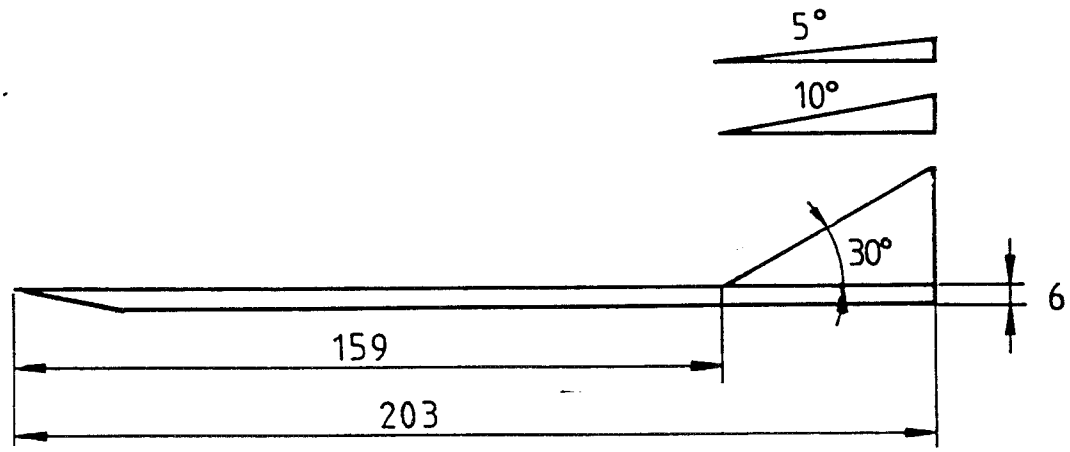

fig. 3.1 Flat plate model with different wedges
All dimensions in mm

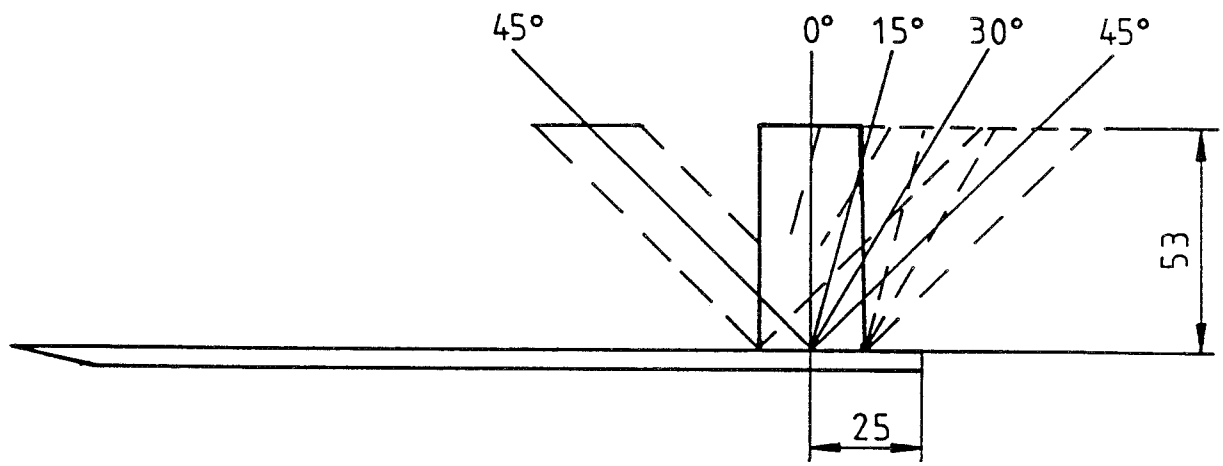

fig. 3.2 Flat plate model with cylinders at 0°, ±15°, ±30°, ±45° sweep angle

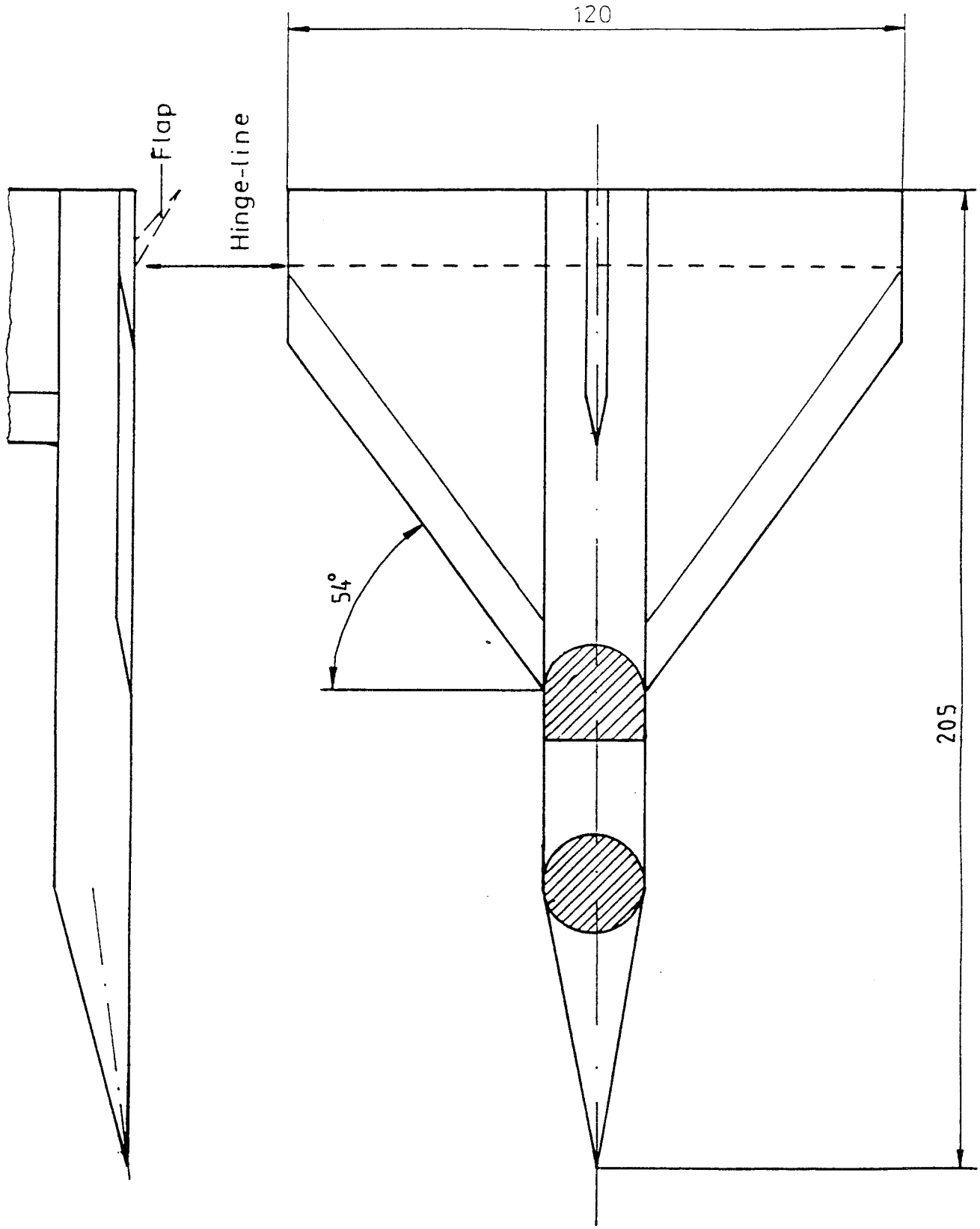

fig. 3.3 Delta wing model

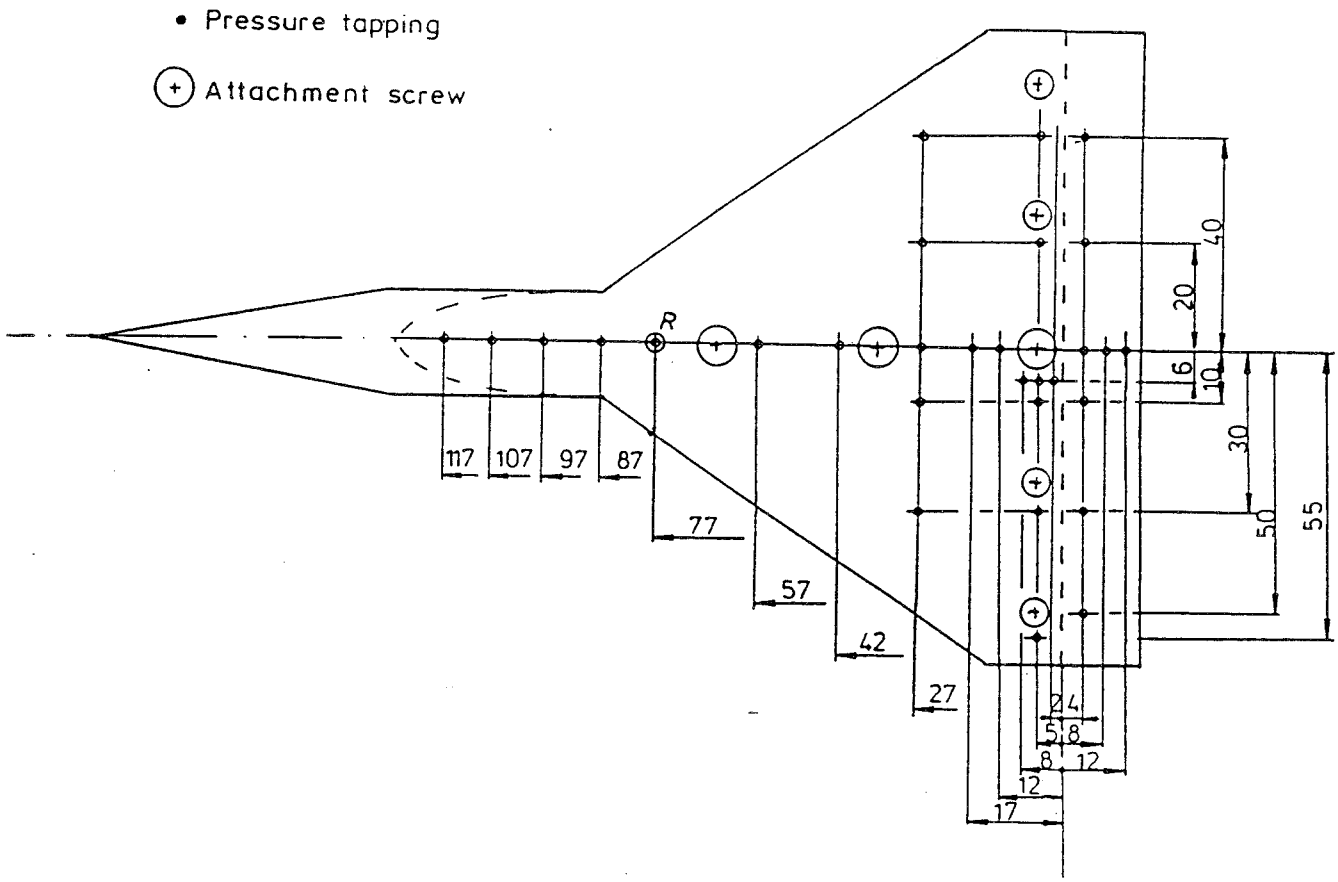

fig. 3.4 Pressure tapping positions on the delta wing model

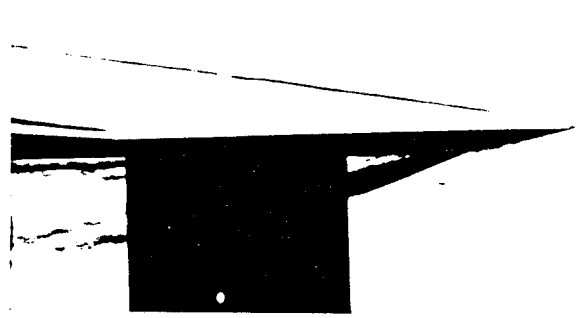

$\alpha = 0°$ $\beta = 5°$

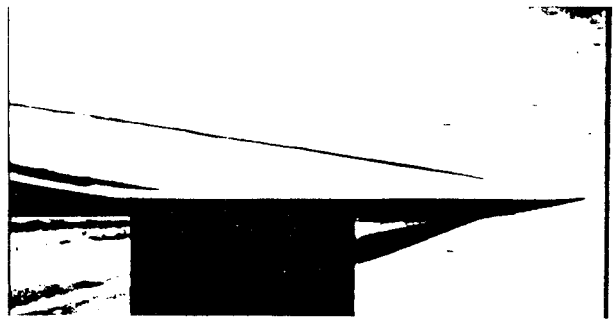

$\alpha = 0°$ $\beta = 10°$

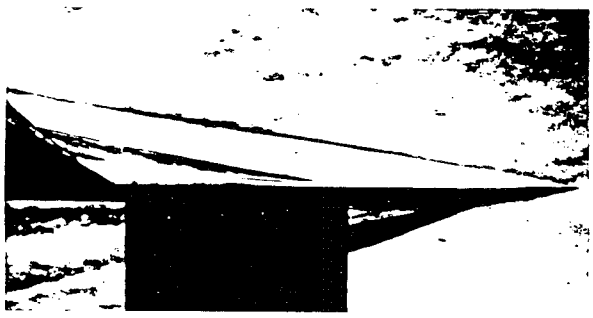

$\alpha = 0°$ $\beta = 30°$

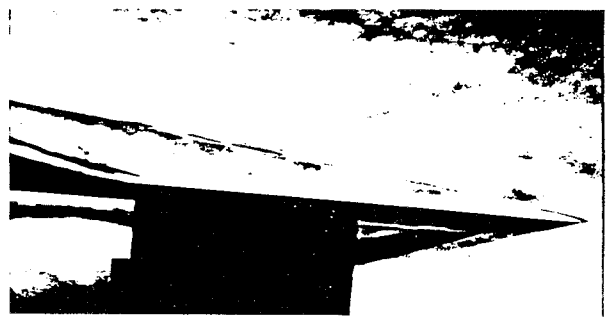

$\alpha = 5°$ $\beta = 10°$

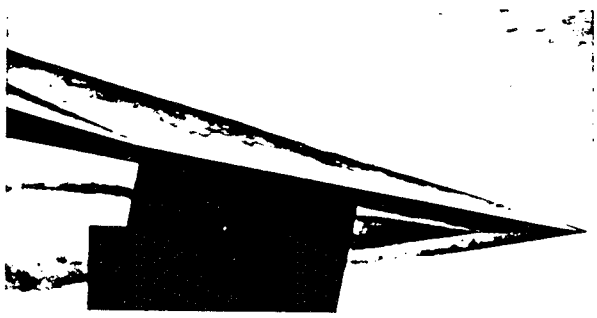

$\alpha = 10°$ $\beta = 5°$

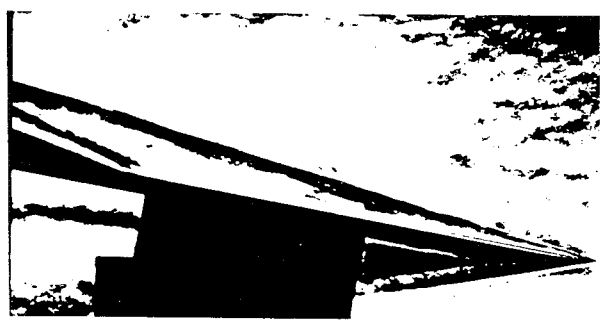

$\alpha = 10°$ $\beta = 10°$

fig. 4.1 Schlieren pictures for two-dimensional corner flow

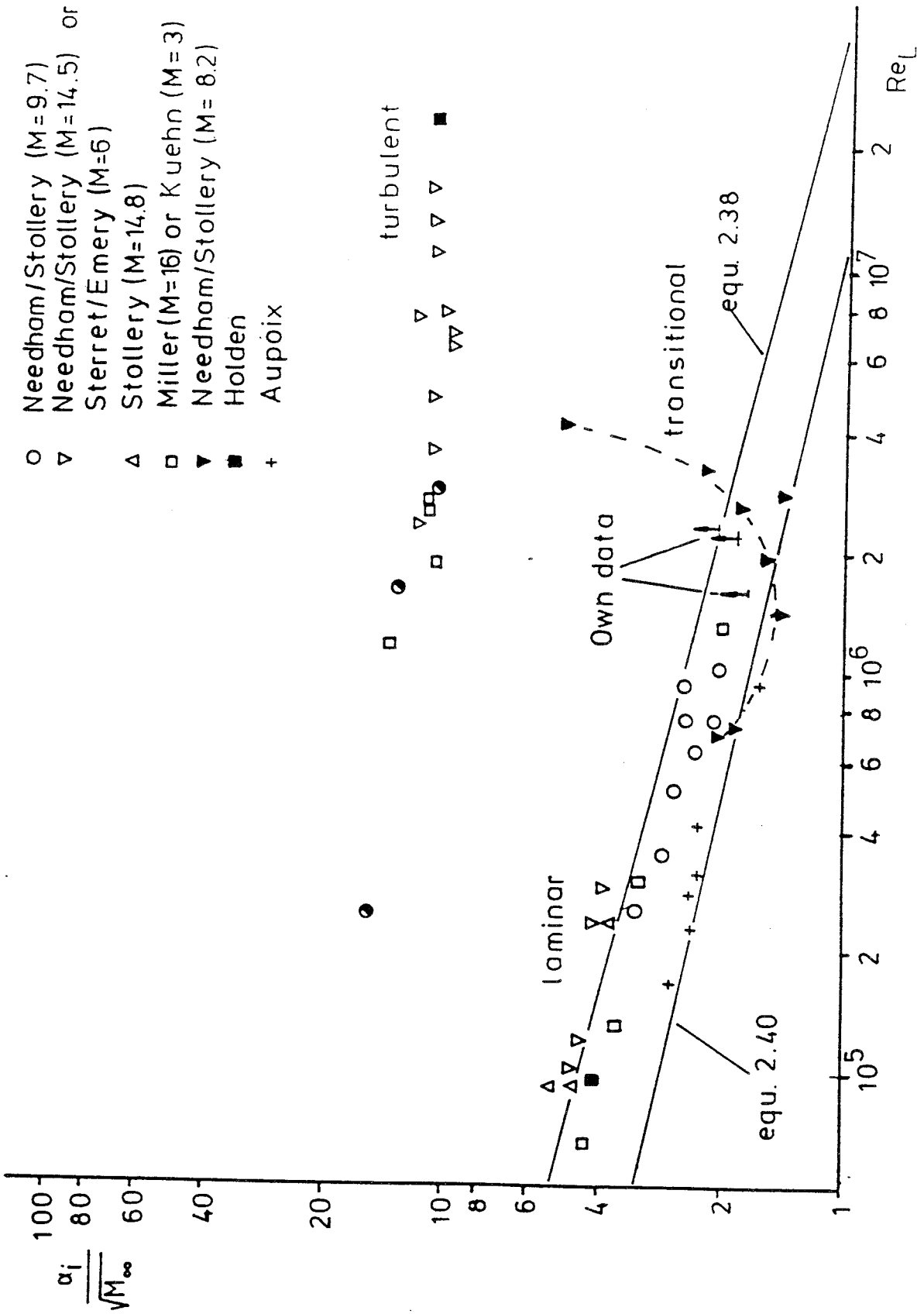

fig. 4.2 Angles for incipient separation for various M and Re numbers (after /13/) compared with own results

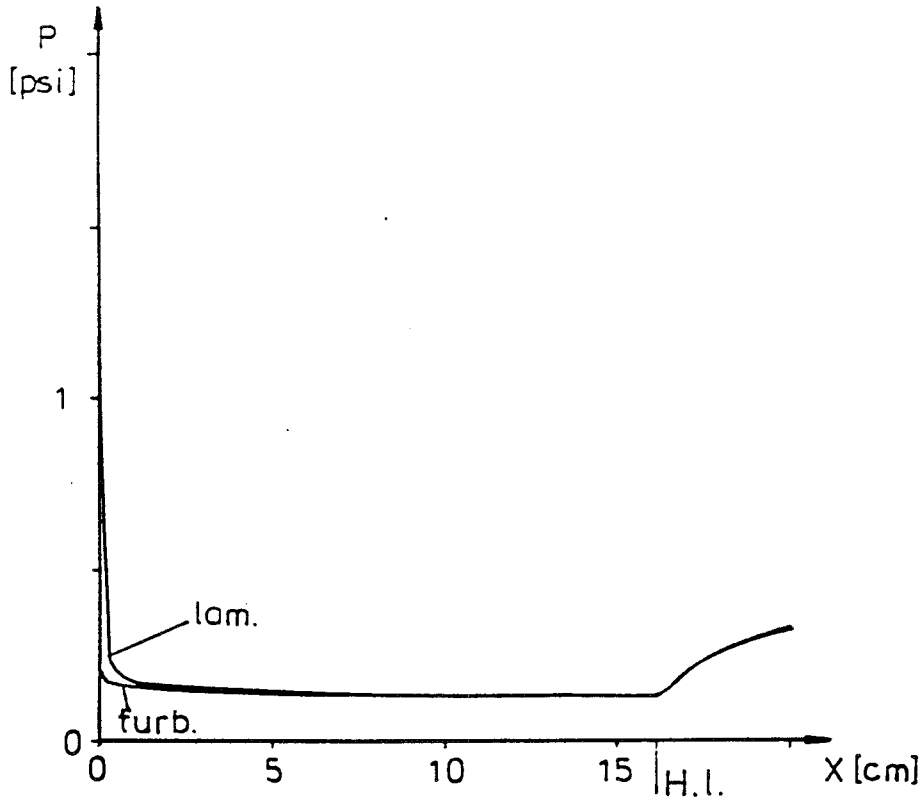

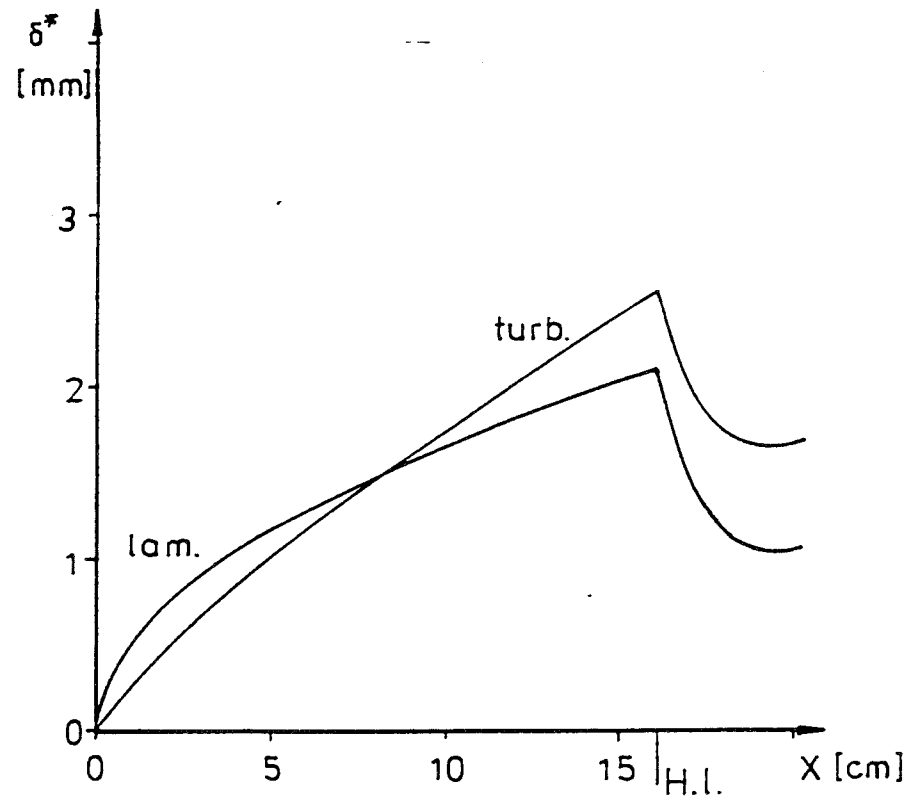

fig. 4.3 Calculation of viscous interaction for a flat plate with a trailing edge flap $\alpha = 0^\circ$ $\beta = 5^\circ$

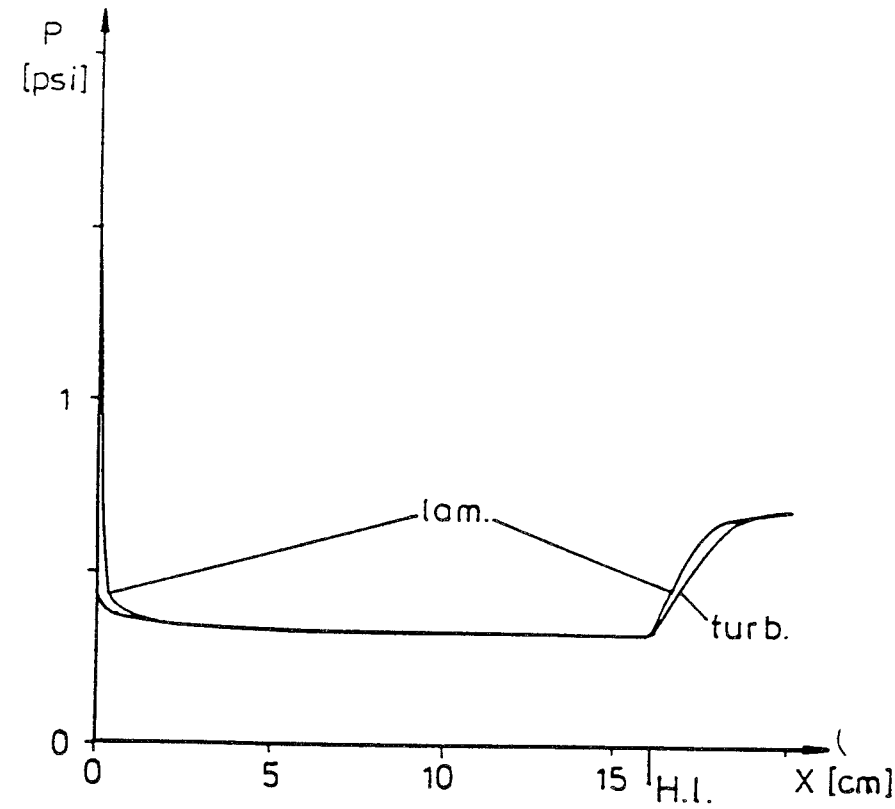

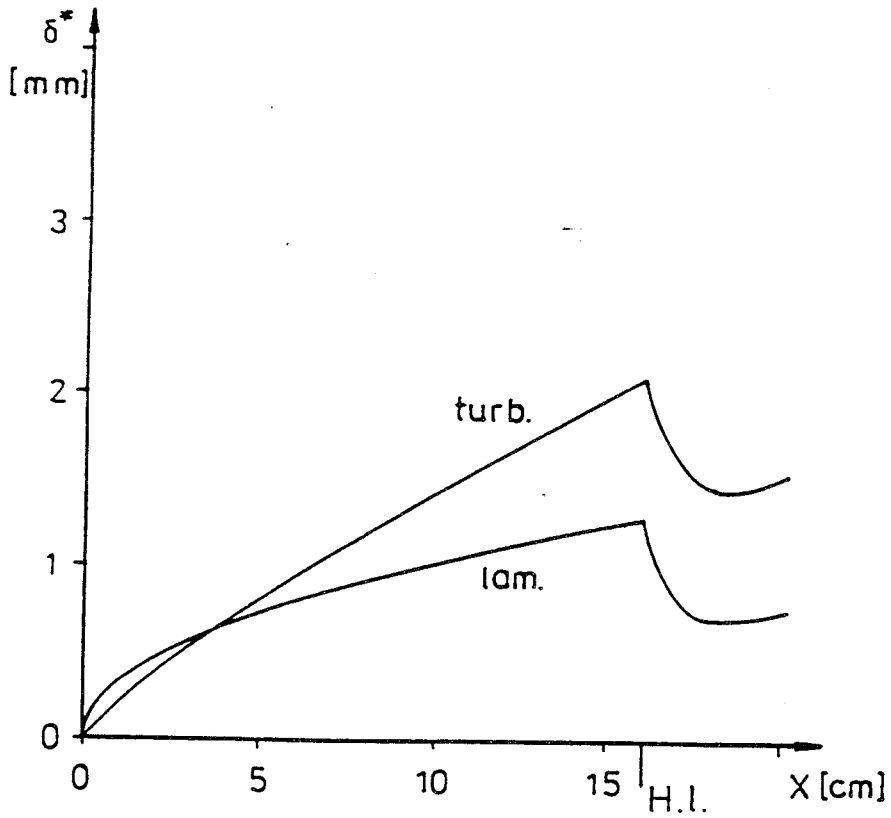

fig. 4.3 concluded $\alpha = 5^\circ$ $\beta = 10^\circ$

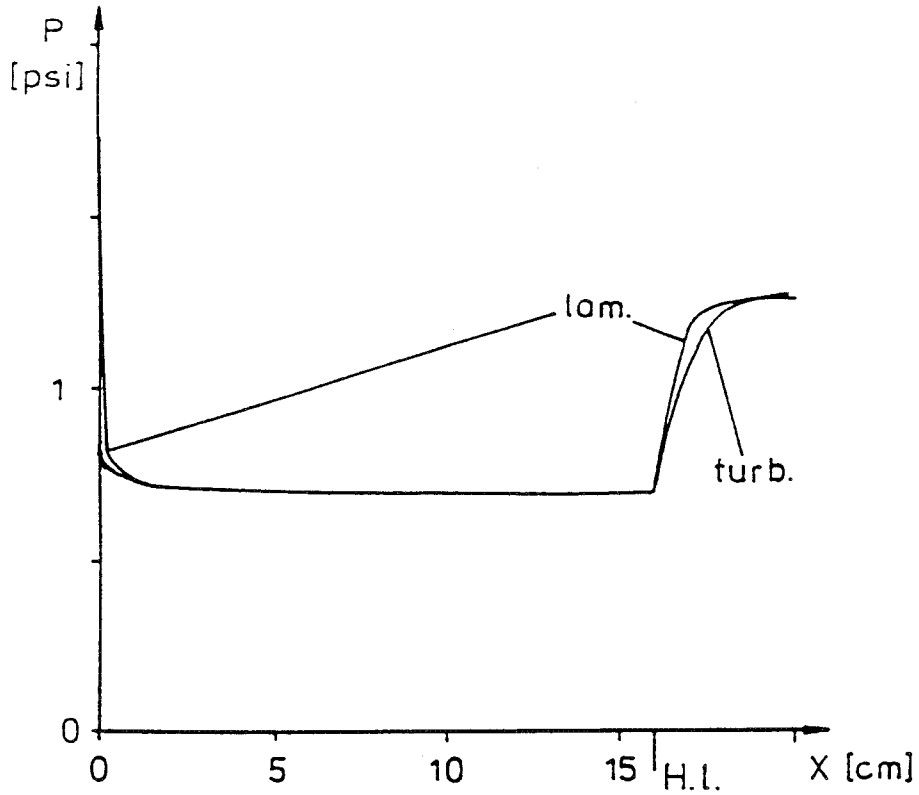

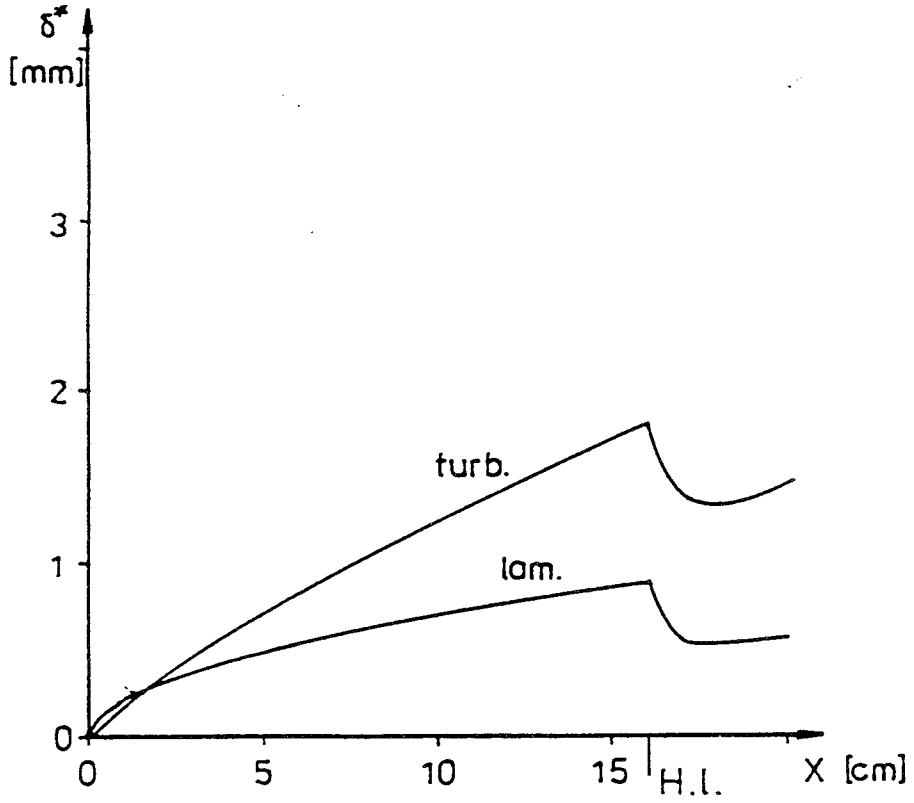

fig. 4.3 concluded $\alpha = 10^{\circ}$ $\beta = 5^{\circ}$

Ψ = 0°

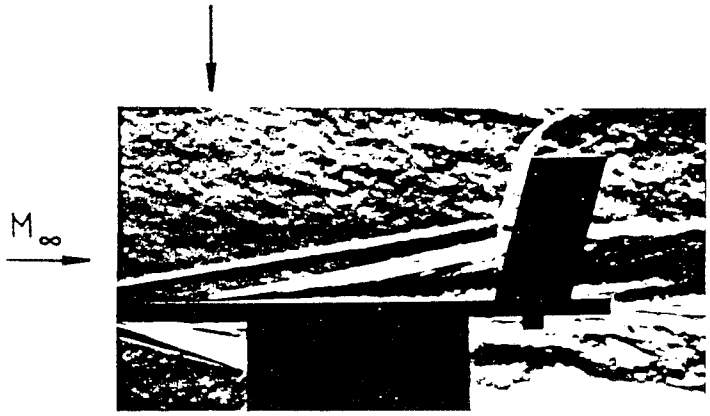

Ψ = 15°

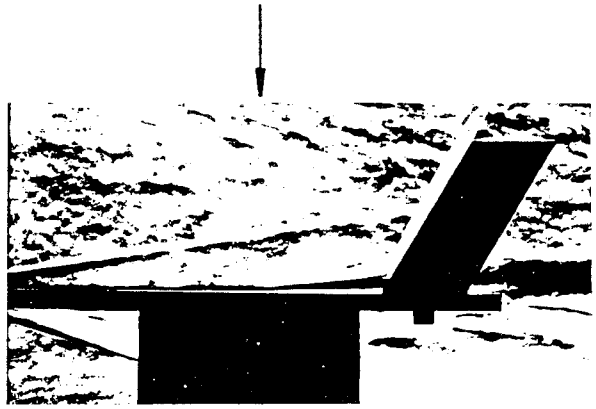

Ψ = 30°

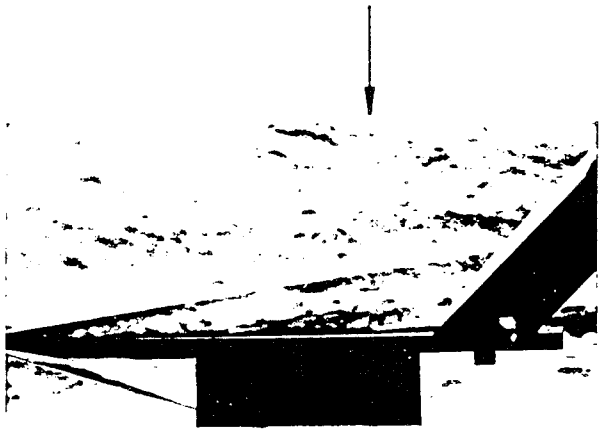

Ψ = 45°

fig. 4.4 Schlieren pictures for flat plate plus backward facing cylinder. The arrow marks the separation point

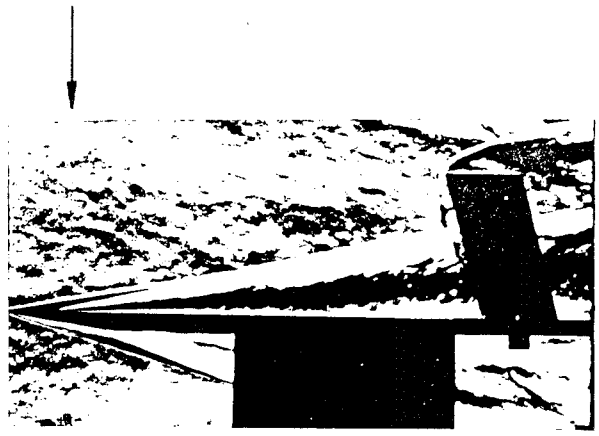

$\Psi = -15°$

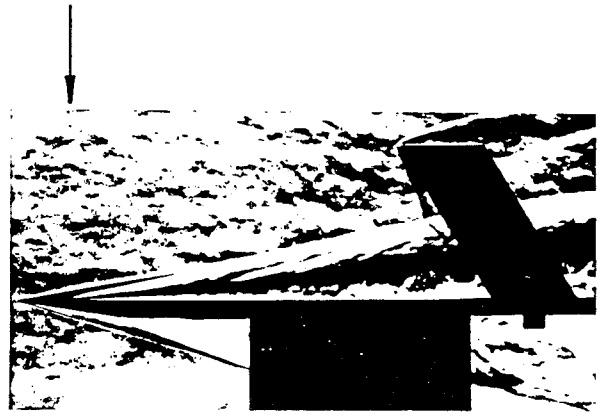

$\Psi = -30°$

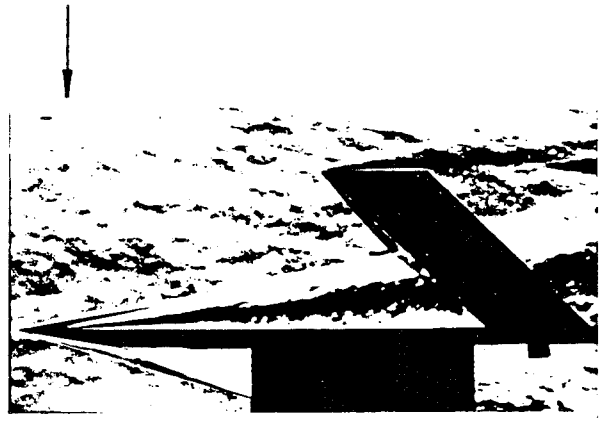

$\Psi = -45°$

fig. 4.4 concluded Forward facing cylinder

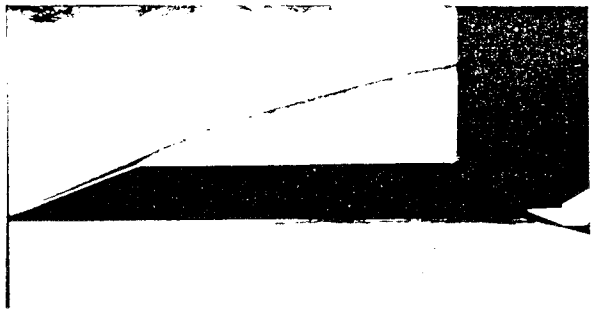

$\alpha = 0°$ $\beta = 10°$

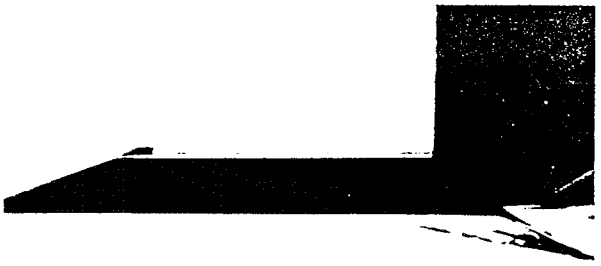

$\alpha = 0°$ $\beta = 20°$

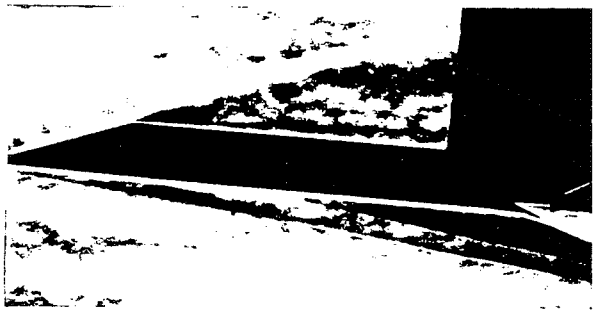

$\alpha = 5°$ $\beta = 10°$

$\alpha = 5°$ $\beta = 20°$

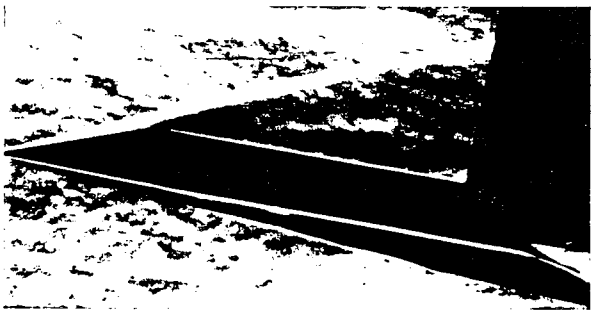

$\alpha = 10°$ $\beta = 10°$

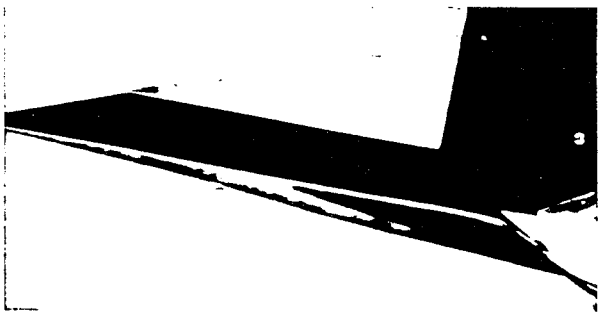

$\alpha = 10°$ $\beta = 20°$

fig. 4.5 Schlieren pictures for delta wing model

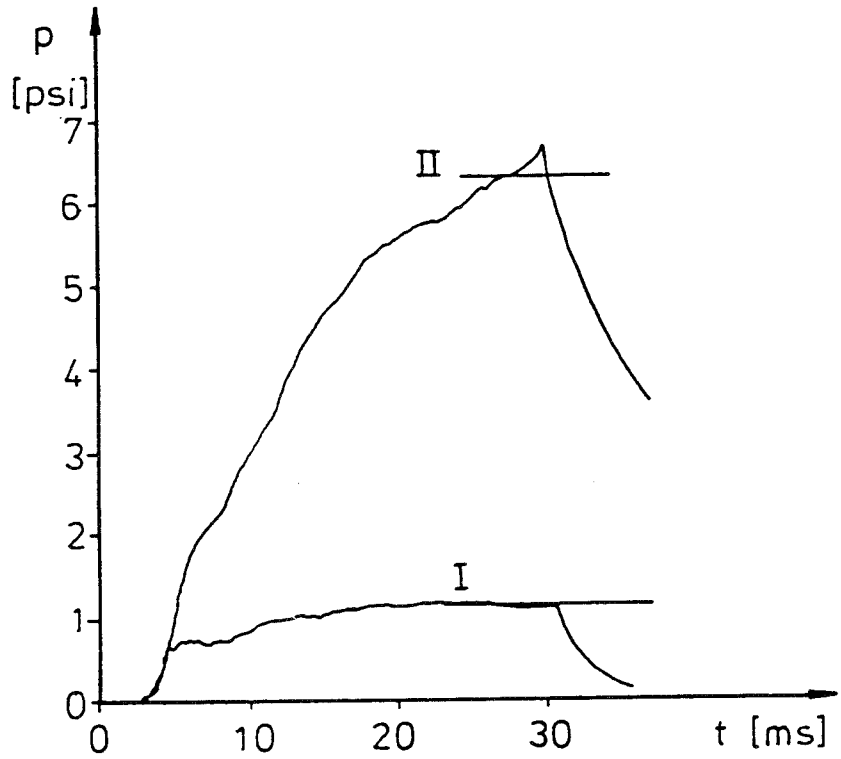

fig. 4.6 Typical pressure signals

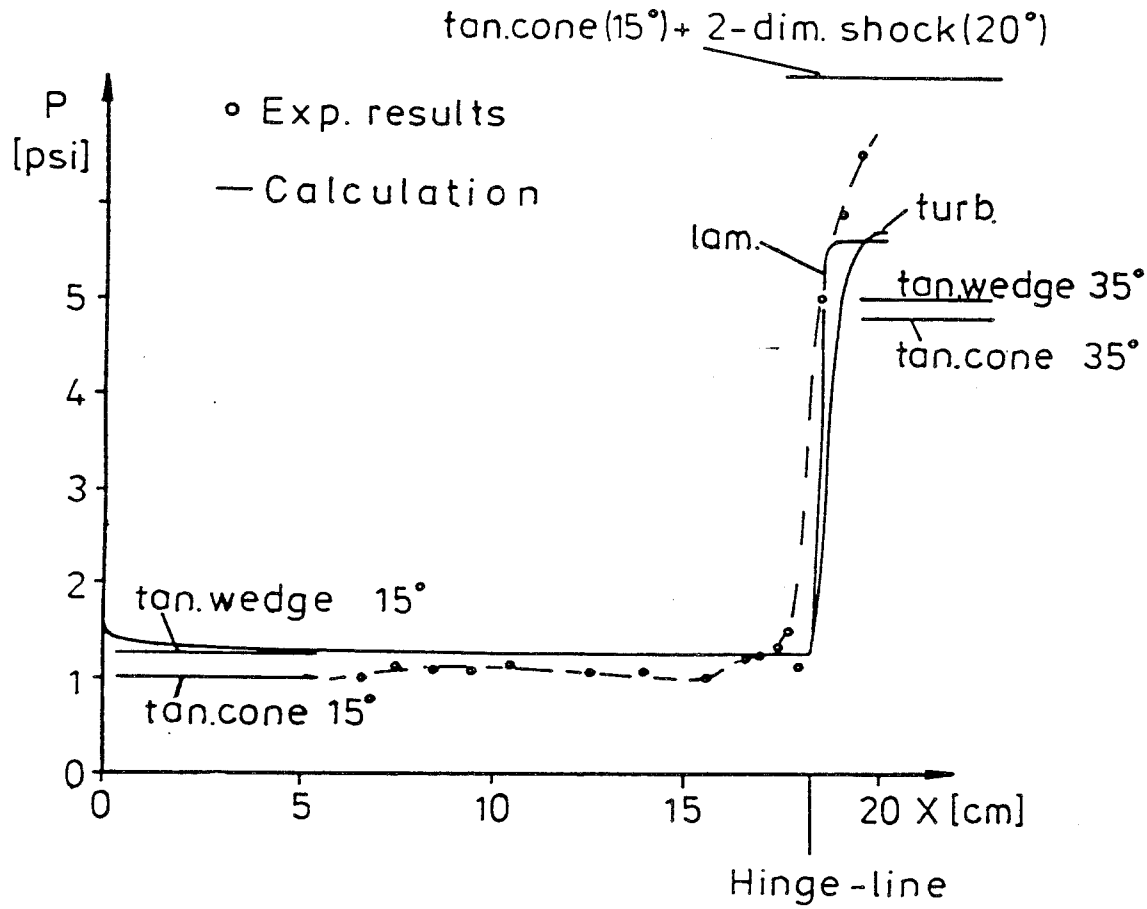

fig. 4.7 Pressure along the centre-line compared with various two-dimensional predictions ($\alpha = 15^\circ$ $\beta = 20^\circ$)

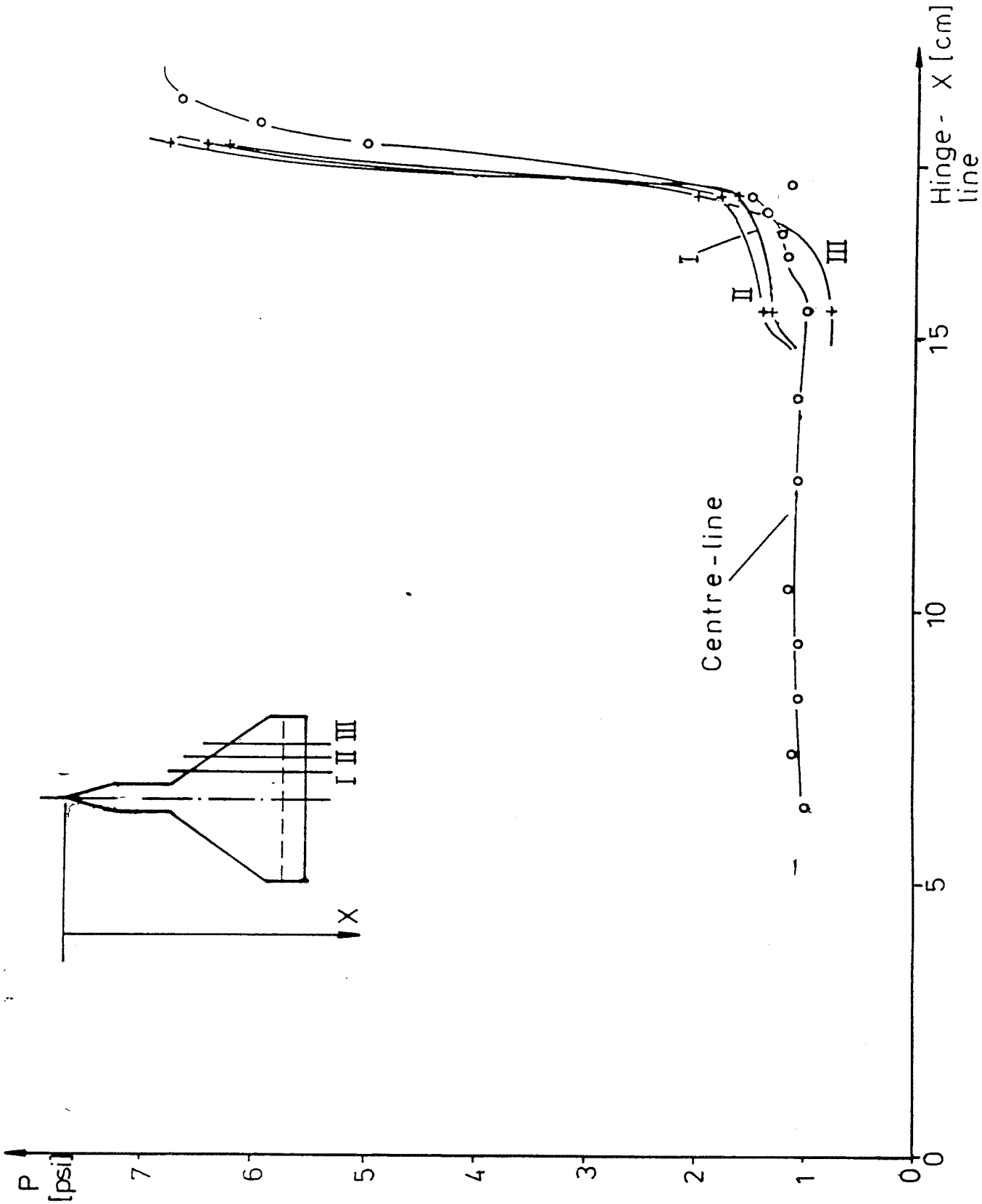

fig. 4.8 Measured pressures for various lines parallel to the centre-line

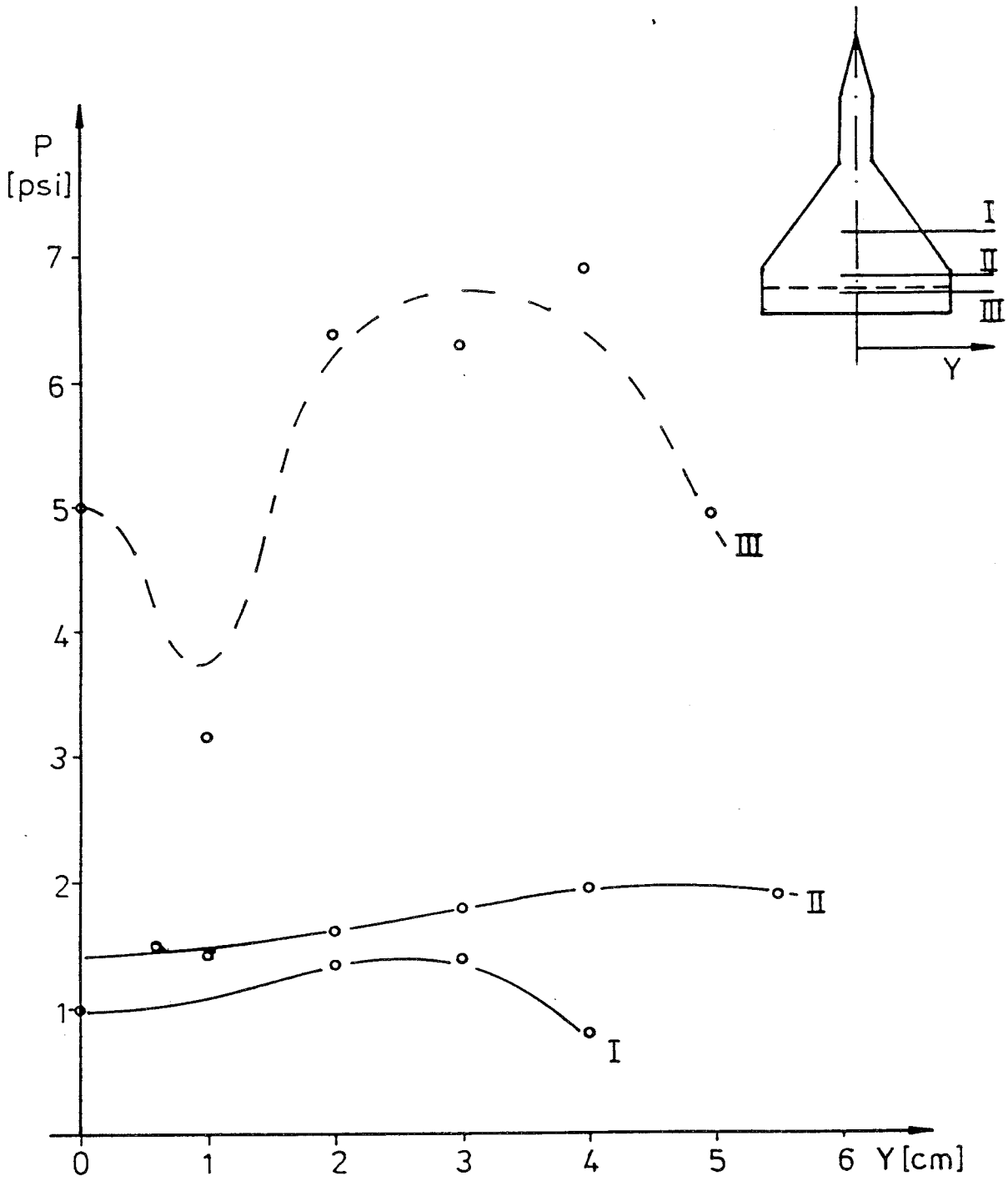

fig. 4.9 Measured pressures along lines perpendicular to the centre-line

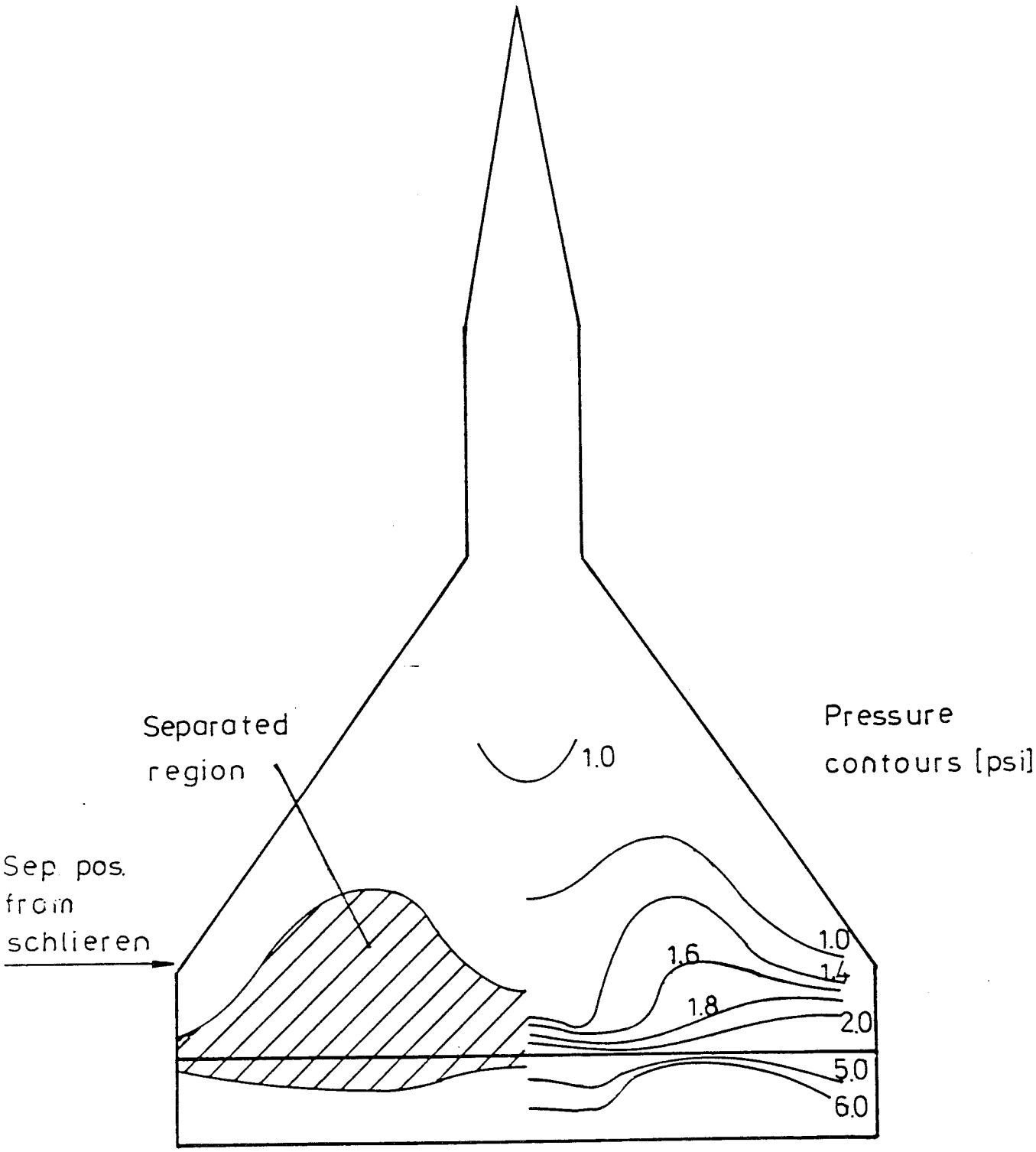

fig. 4.10 Pressure contours and separated region for $\alpha = 15^{\circ}$ and $\beta = 20^{\circ}$

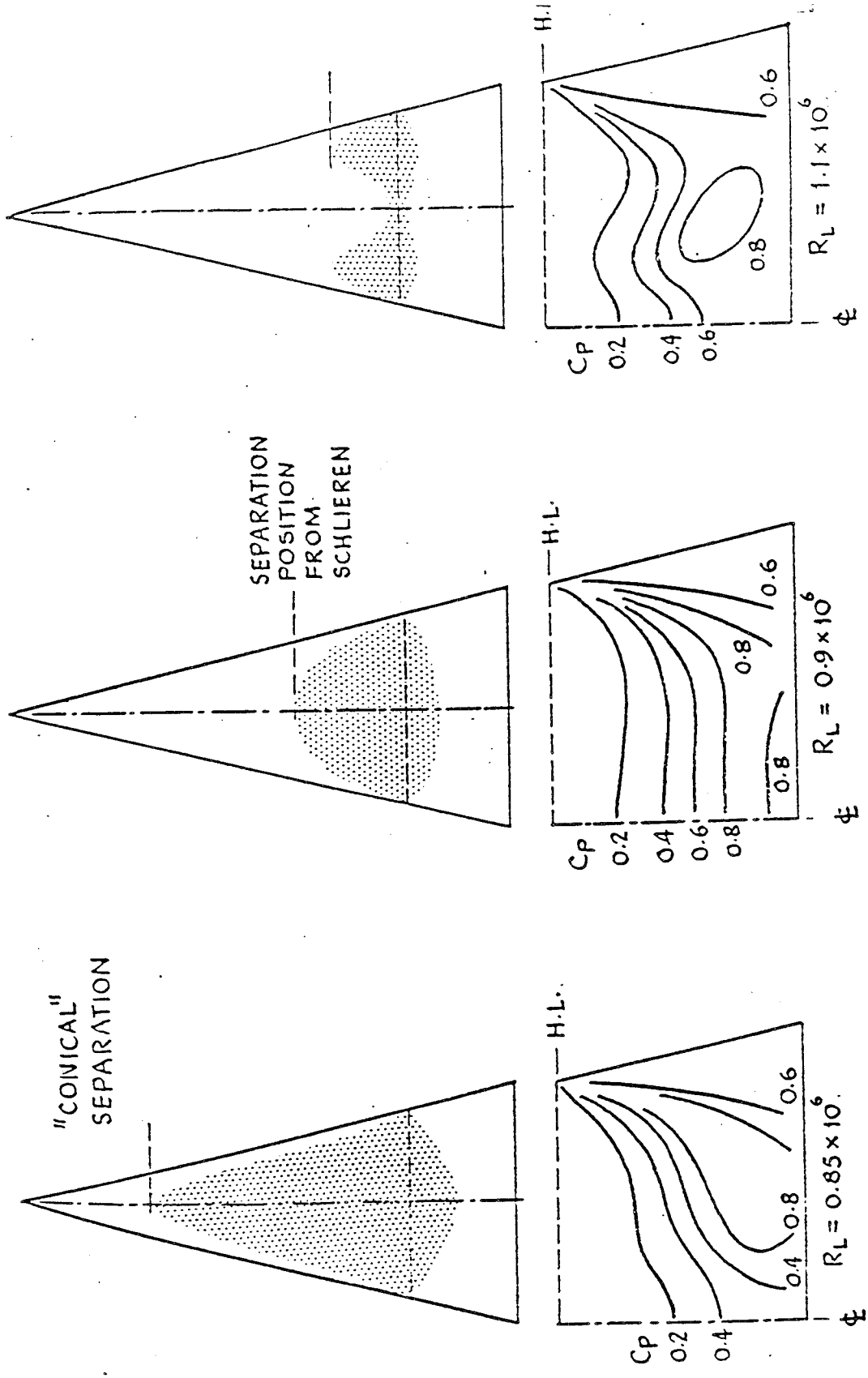

fig. 4.11 Pressure contours and shape of separated region for various Re numbers at $\alpha = 0^\circ$ and $\beta = 30^\circ$ (from /27/)